

# Ca II H and K Chromospheric Emission Lines in Late K and M Dwarfs<sup>1</sup>

Emily Rauscher<sup>2</sup>, Geoffrey W. Marcy<sup>2</sup>

gmarcy@astro.berkeley.edu

## ABSTRACT

We have measured the profiles of the Ca II H and K chromospheric emission lines in 147 main sequence stars of spectral type M5-K7 (masses 0.30-0.55  $M_{\odot}$ ) using multiple high resolution spectra obtained during six years with the HIRES spectrometer on the Keck 1 telescope. Remarkably, the average FWHM, equivalent widths, and line luminosities of Ca II H and K *increase* by a factor of 3 with increasing stellar mass over this small range of stellar masses. We fit the Ca II H and K lines with a double Gaussian model to represent both the chromospheric emission and the non-LTE central absorption. Most of the sample stars display a central absorption that is typically redshifted by  $\sim 0.1$  km s<sup>-1</sup> relative to the emission. This implies that the higher-level, lower density, chromospheric material has a smaller outward velocity (or higher inward velocity) by 0.1 km s<sup>-1</sup> than the lower-level material in the chromosphere, but the nature of this velocity gradient remains unknown. The FWHM of the Ca II H and K emission lines increase with stellar luminosity, reminiscent of the Wilson-Bappu effect in FGK-type stars. Both the equivalent widths and FWHM exhibit modest temporal variability in individual stars. At a given value of  $M_V$ , stars exhibit a spread in both the equivalent width and FWHM of Ca II H and K, due both to a spread in fundamental stellar parameters including rotation rate, age, and possibly metallicity, and to the spread in stellar mass at a given  $M_V$ . The K line is consistently wider than the H line, as expected, and its central absorption is more redshifted, indicating that the H and K lines form at slightly different heights in the chromosphere where the velocities are slightly different. The equivalent width of H $\alpha$  correlates with Ca II H and K only for stars having Ca II equivalent widths above  $\sim 2$  Å, suggesting the existence of a magnetic threshold above which the lower and upper chromosphere become thermally coupled.

*Subject headings:* stars: chromospheres — stars: late-type

---

<sup>1</sup>Based on observations obtained at the W. M. Keck Observatory, which is operated jointly by the University of California and the California Institute of Technology. Keck time has been granted by both NASA and the University of California.

<sup>2</sup>Department of Astronomy, University of California, Berkeley, CA USA 94720

## 1. Introduction

M dwarfs have received considerable attention regarding their internal stellar structure, their atmospheres, and their distribution in the Galaxy (see reviews by Liebert (1994), Burrows et al. (1993) and Bochanski et al. (2005) and references therein). However, their atmospheric structure, dynamics, and magnetic processes remain poorly understood. M dwarfs show clear evidence of chromospheric heating, as revealed by emission lines in optical and UV wavelengths (Giampapa et al. 1989; Gizis et al. 2002; Reid et al. 2002) that constrain models of chromospheric structure (Cram & Giampapa 1987). They also contain hot coronae, as detected by their X-ray emission, with  $L_X/L_{bol}$  up to  $10^{-3}$  (Caillault 1996). Robrade & Schmitt (2005) and others have analyzed X-ray flaring in M dwarfs, and many observations of flaring activity have been made at other wavelengths (Eason et al. 1992; Hawley et al. 2003). Although hot outer atmospheres and flaring activity have been studied in stars of F, G, and K spectral types, M dwarfs deviate from chromospheric/coronal relations found in those stars, indicating a qualitative difference in atmospheric structure, velocity fields, and magnetic morphology (Schrijver & Rutten 1987; Rutten et al. 1989; Valenti & Johns-Krull 2003).

Observations of chromospheres and coronae in M dwarfs have led to models that include significant amounts of nonradiative, magnetic heating in their outer atmospheres (Giampapa et al. 1982; Johns-Krull & Valenti 1996). The observed scatter in X-ray luminosities and chromospheric emission line fluxes can be attributed to temporally changing surface inhomogeneities (Panagi & Mathioudakis 1993) or differences in filling factor between stars (Reid et al. 1995). Mullan & Fleming (1996) showed that acoustic dissipation may provide enough coronal heating for stars dominated by quiet regions, but magnetic heating is required to account for the coronal heating in the more active M dwarfs that likely have sizable covering factors of kilogauss magnetic fields (Johns-Krull & Valenti 1996; Valenti & Johns-Krull 2003).

Here, we probe the atmospheres of M dwarfs with near-UV spectra at the resonant “H and K” transitions of Ca II at 3968 and 3933 Å respectively. We use sufficiently high resolution to resolve structure in the emission line profiles and to extract line widths, asymmetries, and central absorptions. We examine a sample of 147 late K and M dwarfs from spectra previously obtained by the California and Carnegie Planet Search. Multiple spectra for each star yield mean values over time and any temporal changes. We compare the Ca II H and K lines to H $\alpha$  equivalent widths, providing a tie to coronal gas.

In Section 2 we describe the stellar sample and the Keck spectra. In Section 3 we describe the double Gaussian model of the lines. In Section 4 we present the resulting observed line parameters, and in Section 5 we offer discussion and summary.

## 2. Observations

All spectra used in this study were taken from the California and Carnegie Planet Search Program, with a set-up described by Wright et al. (2004) and briefly summarized here. From 1997-2004, the Planet Search Program has been monitoring the velocities of 700 FGKM stars with the goal of detecting extrasolar planets, as described by Butler et al. (1996). The spectra were all obtained with the HIRES spectrometer at Keck Observatory (Vogt et al. 1994). They span the wavelength region, 3850 to 6200 Å with a resolution of  $R=55,000$  corresponding to a spectrometer PSF with  $\text{FWHM} = 5.5 \text{ km s}^{-1}$  or 2.8 pixels (24  $\mu$  each) on the CCD. Exposure times of typically 8 minutes yield a signal-to-noise ratio of 60 per pixel in the continuum around the Ca II H and K lines for the majority of the M dwarfs, most having  $V=9-11$  studied here. But the quality can be higher or lower depending on seeing and B-V of the star. The spectra are not flux-calibrated.

The stars included here are those from the Planet Search Program having  $B-V > 1.3$  corresponding to a spectral type of about K7. All colors were taken from the Hipparcos catalogue (ESA 1997). They were originally selected for that search by sieving the Gliese Catalog and Hipparcos catalog for late K-type and M dwarfs that were both brighter than  $V = 11.5$  and devoid of known stellar companions within 2 arcsec, to avoid contamination at the spectrometer slit. The stars were chosen without regard to previously known emission lines in their spectra. Indeed, most such stars exhibit emission at Ca II H and K (but not necessarily at H $\alpha$ ). Thus, this present sample is representative of the single, K7-M5 dwarfs within  $\sim 15$  pc, though some are slightly farther away.<sup>1</sup> The limit at spectral type M5 stems largely from their faintness for the purposes of high resolution spectroscopy, most such stars being fainter than  $V = 11.5$ .

The resulting sample of 147 stars is shown plotted in a color-magnitude diagram in Figure 1. The stars departing farthest from the main sequence are labeled, with the departures due most likely to stellar companions, extraordinary metallicity, or simply to poor photometry. The width of the main sequence in Figure 1 indicates the limited value of B-V as a diagnostic for  $T_{\text{eff}}$  for M dwarfs, due to its sensitivity to metallicity caused by line blanketing (Gizis 1997). Table 1 lists for each star its common names, spectral type,  $M_V$ , B-V, the number of observations, and the time range over which it was observed.

We obtained a total of 2408 spectra for the 147 stars. Each spectrum was reduced as part of the planet-search automated pipeline. The raw CCD images were biased-subtracted, the flat-fielding was done with a quartz lamp through the same spectrometer setup, the spectral order locations were mapped and fitted with a third order polynomial, and the final one-dimensional spectra were extracted by summing along the column within each order. These spectra give the number of photons in each pixel of width  $2 \text{ km s}^{-1}$ .

---

<sup>1</sup>Other exceptions stem from slight errors in photometry, notably HD 90875 that had a B-V color originally mislabeled as 1.70. It is actually spectral type K5.

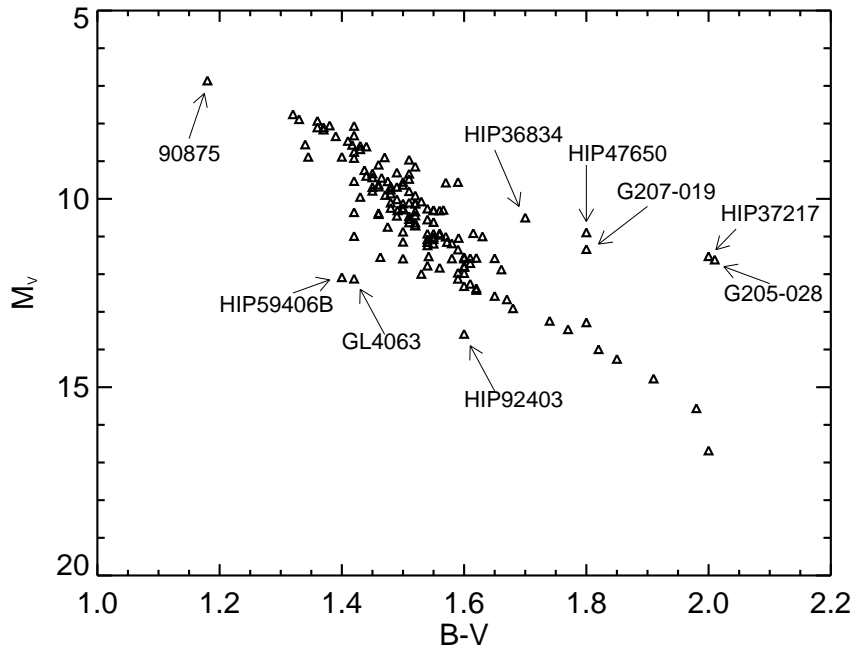


Fig. 1.— The color-magnitude diagram for the 147 K7-M5 dwarfs in the stellar sample.

### 3. Analysis

Inspection by eye of the Ca II H and K emission line profiles from the 147 late-K and M dwarfs reveals considerable structure. The widths of the Ca II H and K emission lines in the K7-M0 dwarfs are clearly wider than those of the M1-M5 dwarfs. Many emission lines are double-peaked, reminiscent of the central “absorption” reversal well known to exist in Ca II H and K profiles of G and K dwarfs. Many M dwarfs that do not exhibit double peaks appear to have flat-topped emission lines, as if weak central absorption were suppressing the peak of the emission. Also visible to the eye are asymmetries in the double-peaked emission profiles, with the central absorption being shifted redward relative to the emission. The blueward peak is almost always taller than the redward one, providing a sensitive measure of relative Doppler shift of the emission and central absorption. The Ca II H and K profiles stem from the non-LTE line transfer and velocity fields in the low density chromospheres of M dwarfs. The central absorption stems from the dependence of the source function on height in the optically thick chromosphere rather than from actual absorption. The variety of visible structure in the line profiles calls for quantitative measurements, in advance of future modeling of the line transfer.

Our analysis of the Ca II H and K lines was performed by fitting them with the sum of two Gaussian curves. We tried other functional forms, such as flat topped functions,

but the double-Gaussian yielded the smallest value of  $\chi^2$  and (remarkably) reproduced all off the observed structure in the line profiles. The model consisted of a positive Gaussian representing the chromospheric emission that emerges from the broad bottoms of the photospheric Ca II absorption features. Added to that is a second Gaussian of negative amplitude representing non-LTE “absorption” at line center. A constant background level was left as a final parameter, representing the base of the photospheric absorption. The height, width, and central position of both Gaussians were free to vary as well as the background level, for a total of 7 parameters used to minimize  $\chi^2$ . This model provides excellent fits to those emission lines that exhibit either obvious central absorption or flat tops. For those emission lines without an obvious central absorption, we found that the double Gaussian commonly fit the line profiles well, especially at the top, better than did a single Gaussian.

Figure 2 shows our model fit to the H and K lines from spectra of three stars, illustrating different line shapes: obviously double-peaked lines, flat-topped lines, and thin lines. In each case the emission Gaussian alone fits the edges of the line but overshoots the top, which can then be accommodated by the second Gaussian of negative amplitude.

From these fits we derived a set of parameters for each line including the equivalent width (EW), the full width at half maximum (FWHM), and the wavelength difference between the centers of the two Gaussians ( $\Delta\lambda_c$ ), indicating a relative Doppler shift between the emission and absorption. For those profiles that were clearly double-peaked, we determined the ratio of the maximum counts in the blue peak to the maximum counts in the red peak (V/R). The equivalent width was determined by dividing the area in the line by the continuum around the line. The area under the line was easy to measure. We subtracted the constant background found by our fit from the line and integrated the counts within the line.

The continuum determination presented challenges. The spectra of M dwarfs in this region contain many absorption lines, leaving no obvious choice for a constant value to assign to the continuum. We determined a continuum value by averaging the number of counts within two wavelength bins located on either side of the broad photospheric H line, as shown in Figure 3. These continuum regions are analogous to those used in the determination of the well-known Mt. Wilson  $S$  values. (The locations of these ranges were set with reference to the center of the emission line so as to be constant within the rest frame of each star.) We performed a spline on the double-Gaussian fitted curve to find the width at half of the background-subtracted maximum.

We used  $\Delta\lambda_c$  and V/R as measures of the asymmetry of the lines. We defined  $\Delta\lambda_c$  as the center of the absorption Gaussian in our model minus the center of the emission Gaussian, so that a value greater than zero corresponds to a redshifted absorption relative to the emission. As previously used by Smith & Shetrone (2004), V/R is only applicable for double-peaked lines, i.e. those with a visible absorption at line center. For these lines, we found the ratio of the maximum number of counts in the blue side of the emission line to that on the red side. Lines having a blue peak higher than the red peak (as typically seen here) have V/R > 1. Segregation of red and blue peaks was formally made (without operator intervention) using the location of the center of the emission Gaussian. The parameter  $\Delta\lambda_c$  is applicable

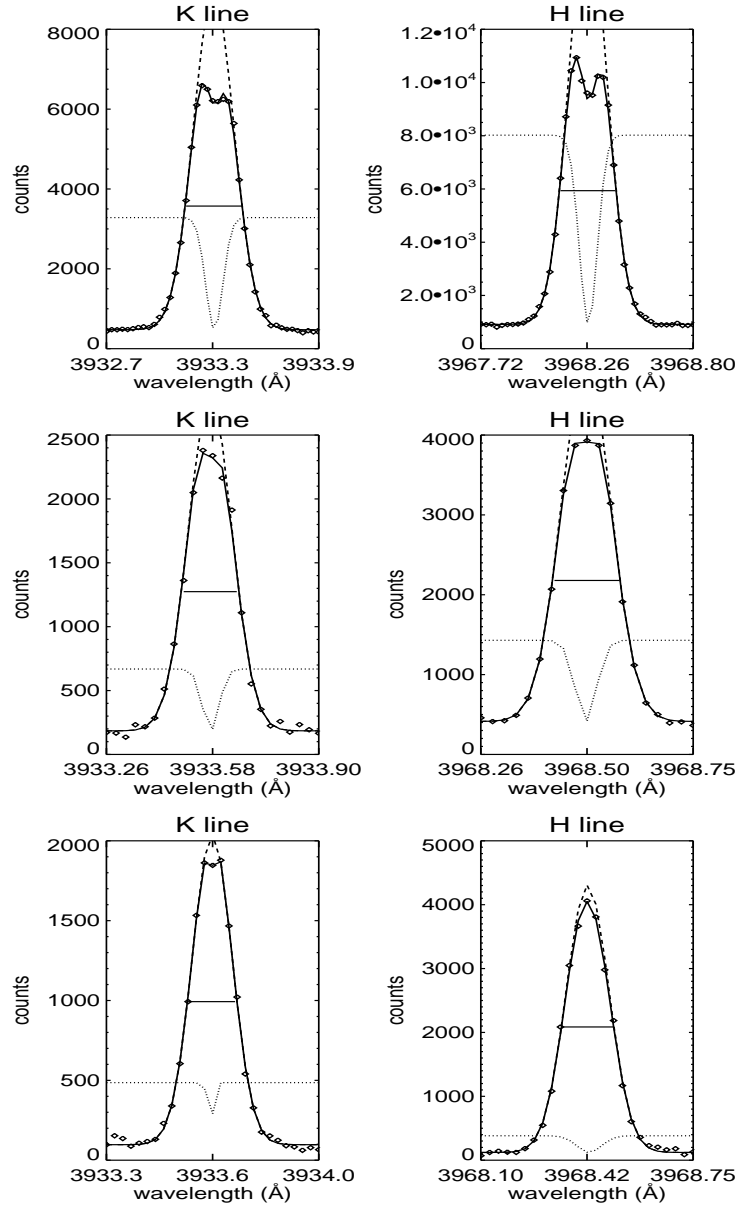


Fig. 2.— Representative observed Ca II H and K profiles (dots) and the double-Gaussian model fits (solid line) to them, for three stars. The two separate Gaussians (emission and absorption) are plotted as dashed and dotted lines, respectively. Note that for flat-topped lines, the negative Gaussian serves to produce an adequate fit. The FWHMs are shown for each line as a horizontal line at the mid-height. Top spectrum is of GJ 809, middle spectrum of GJ 251, and bottom spectrum of GJ 406.

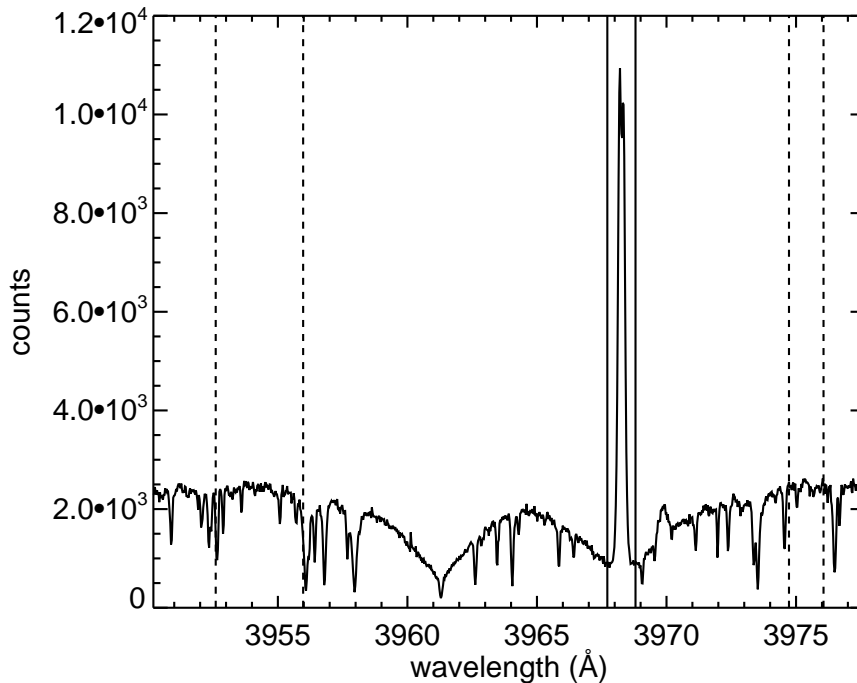


Fig. 3.— A representative spectrum (from GJ 809), showing the Ca II H line emission and the continuum in its vicinity. The two vertical solid lines mark the wavelength region used for fitting the emission line. The two pairs of vertical dashed lines mark the wavelength ranges used to measure an average continuum value. Peculiar to this spectrum is the visible presence of H $\epsilon$  emission at 3970 Å, just redward of the H line.

to more stars than was V/R since it can be calculated for any line, whereas V/R requires a double-peaked line. Only 40% of the stars here were double-peaked.

Our automated fitting procedure occasionally failed to find good fits to the H and K lines in our 2408 spectra. The process obtained good fits for both of the lines for 63% of the spectra and was not able to find a good fit for either line in 15% of the cases. In many cases the poor fits were simply due to spectra of such low signal-to-noise ratio that the  $\chi^2$  minimization algorithm failed. Since we had multiple observations of each star, we ignored the poorest fits from our subsequent analysis.

Four stars had no adequate fit of either line, with  $\chi^2$  well above unity. Two of them, L 758-107<sup>2</sup> and GL 745B, have emission lines that were too weak to fit with any integrity. The other two, GL 388 and HIP 112460, have very strong H and K lines, but the reduced  $\chi^2$  values were above 10 due to their distinctly non-Gaussian profiles, and therefore we consider

---

<sup>2</sup>This star is internally referred to as HIP 59406B.

these fits dubious. Of the 147 original stars, 136 have at least one good measurement of both the H and the K lines, and another 7 stars have a good quality measurement of at least one line.

## 4. Results

From each spectrum of the H and K lines for each star, we compiled the mean values of the best-fit parameters and their standard deviations. The latter is a measure of internal precision and temporal variability, to be discussed in each subsequent section. Tables 2 and 3 list the final measurements for the H and K lines, respectively, for each star. Columns 1-3 list the common names of each star, and column 4 gives the number of spectra analyzed with good fits. Columns 5 and 6 give the equivalent width and its standard deviation. Columns 7 and 8 give the FWHM and its standard deviation. Columns 9 and 10 give  $\Delta\lambda_c$  and its standard deviation and columns 11 and 12 give the mean and standard deviations for  $V/R$ .

Ideally, one would like to measure chromospheric parameters as a function of stellar mass. Unfortunately, we do not have secure photometric calibration of stellar mass for M dwarfs that would be immune to variations in chromospheric activity. Nor do we have a mass calibration immune to the unknown metallicities of the stars. Thus B-V and  $M_V$  remain as modest proxies of stellar mass here, with due concern about their integrity as such. We proceed to examine how the measured chromospheric parameters depend on  $M_V$  which is likely a better proxy for mass than B-V. Clearly there is a great need for accurate masses for M dwarfs.

### 4.1. Equivalent Widths and Line Widths of Ca II H and K

Previous studies of M dwarfs have reported measurements of either line fluxes (Robinson et al. (1990), Panagi & Mathioudakis (1993)) or equivalent widths as the diagnostics stellar activity, most often using unresolved lines. As our spectra are not flux calibrated, we report the equivalent width of the Ca II H and K lines, obtained from the double-Gaussian fit. Such measurements are explicitly dependent on the color, and hence  $M_V$  and mass, of the star. The nearby UV continuum decreases with increasing color and lower mass. Thus for a fixed luminosity in the lines, the Ca II H and K equivalent widths would increase with increasing stellar color, simply due to the decreasing continuum.

Figure 4 shows the measured values of EW for the Ca II H and K lines (diamonds and crosses, respectively) versus  $M_V$ . The figure shows that the EWs of Ca II H and K for late K and early M dwarfs ( $M_V = 7-9$ ) are typically  $\sim 1 \text{ \AA}$ . However, the later type M dwarfs ( $M_V = 9-13$ ) have smaller EWs of Ca II H and K, typically  $\sim 0.3 \text{ \AA}$ . Thus, the EW of Ca II H and K increases by a factor of 3 toward decreasing  $M_V$ , and thus toward higher stellar mass. The increase in EW with stellar mass is in the opposite direction from that which would be

caused simply by the increasing UV continuum flux with stellar mass. *Thus, the luminosity in the Ca II H and K lines increases, by at least a factor of 3, with increasing mass from M5 to K7.*

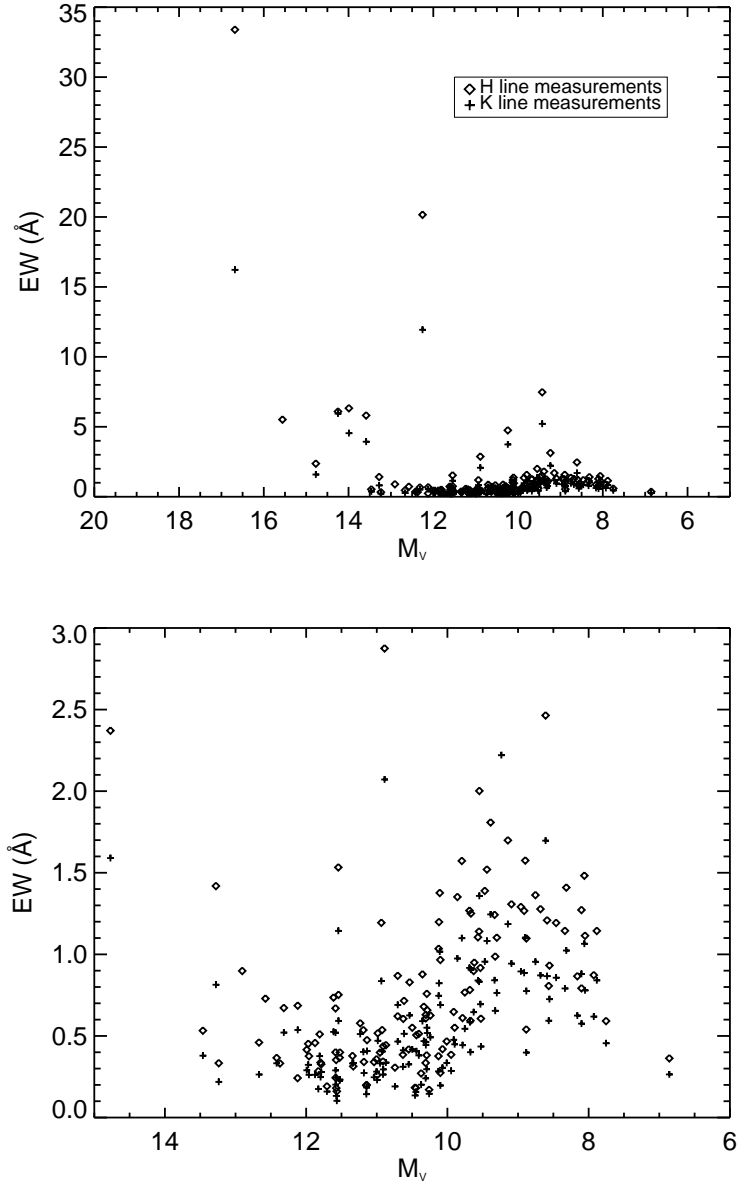


Fig. 4.— The mean EW of Ca II H and K for each star versus its  $M_V$ . Top: All stars. Bottom: a close-up of the majority of stars that have  $EW < 3 \text{ \AA}$ . The errors of  $\sim 0.025 \text{ \AA}$  are less than the size of the symbols.

Of some interest is the transition from partially to fully convective stars that is expected to occur near  $0.3 M_{\odot}$  (Burrows et al. 1997). Indeed, Gizis et al. (2002) found an increased level of activity (as measured by H $\alpha$  EWs) at M2.5/3, which corresponds roughly to this mass. Mathioudakis & Doyle (1991) and Fleming et al. (1995) note that  $0.3 M_{\odot}$  (where full convection sets in) may correspond to spectral types M4-M5. It is tempting to associate the remarkable factor of 3 rise in the chromospheric H and K lines seen here with a dynamo explanation. Such an explanation may be appropriate. Note, however, that Gizis et al. (2002) found an increase in H $\alpha$  EW for later type stars while here we find a decrease in the Ca II H and K emission for those stars. Nonetheless, Figure 4 does not reveal a sharp discontinuity in EW at any  $M_V$ . Thus we find no convincing evidence of a discontinuous change in the dynamo in the domain K7-M5.

Since the plotted values of EW are the means of multiple measurements for each star, we can compare the vertical spread of the points to the standard deviations seen for each star individually. The standard deviations of EW (listed in Tables 2 and 3) are typically  $\sim 0.1 \text{ \AA}$  while the spread in EWs at any given  $M_V$  is much larger. Thus it appears that the spread in EW at a given  $M_V$  is greater than can be accounted for by temporal variability. The observed spread may be caused by the degeneracy in mass at a given  $M_V$ ; however, we suspect that this degeneracy alone is not adequate to account for all of the spread. Rather, the chromospheric activity of a star is likely influenced by other stellar parameters, notably rotation, that vary from star to star at a given mass. Indeed similar analysis in H $\alpha$  emission has shown that activity is related to both age and rotation (Stauffer et al. 1997), which is likely the cause of variance of Ca II emission as well.

The FWHM of the Ca II H and K emission lines is plotted in Figure 5 versus  $M_V$ . This plot shows a tight relation between Ca II H and K line width and  $M_V$ , such that FWHM increases with brighter  $M_V$  and hence with stellar mass. This is reminiscent of the Wilson-Bappu effect in FGK stars as discussed in Giampapa (1994) and modeled by Ayres (1979), where the logarithm of the width of chromospheric emission lines is observed to increase linearly with decreasing absolute magnitude. This remarkably tight relationship between line width and  $M_V$  for M dwarfs is not understood, to our knowledge. The conventional Wilson Bappu effect in FGK stars represents a correlation between emission line width with luminosity which in turn is directly related to evolutionary state (luminosity class) and hence surface gravity. In contrast, the M dwarfs all reside nearly on the main sequence, none having evolved at all, albeit having different masses, radii, and gravities. Nonetheless, it is apparent that the Ca II H and K line width in M dwarfs could similarly serve to determine distances. Ultimately, a line-transfer explanation of the Wilson-Bappu effect in M dwarfs must include the variation of chromospheric pressure and mass column as a function of stellar mass.

Slight inflections are visible in Figure 5, but the limitations discussed earlier associated with the use of  $M_V$  as a proxy for stellar mass may be the cause.

Figure 5 exhibits a lower limit of  $9 \text{ km s}^{-1}$  for the observed FWHM of the Ca II H and K lines. This limiting width represents the convolution of the lowest intrinsic line widths and the width of the PSF of the spectrometer,  $5.5 \text{ km s}^{-1}$ . Thus, considering a quadrature sum

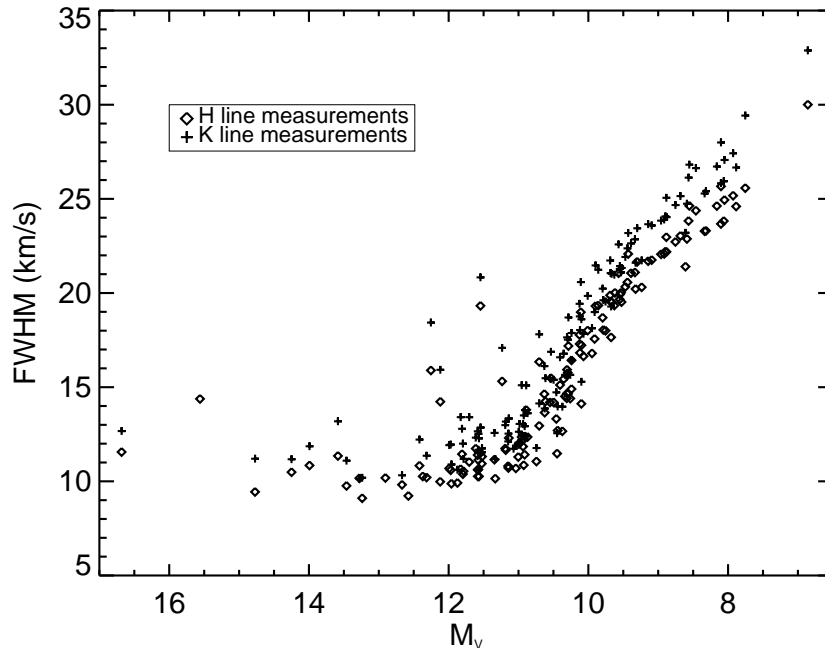


Fig. 5.— The mean FWHM of the H and K lines for each star as a function of  $M_V$ . The FWHM increases with brighter  $M_V$ , in a remarkably tight correlation. The FWHM increases by a factor of  $\sim 3$  from over this narrow range in spectral types, M5-K7. This correlation is reminiscent of the Wilson Bappu effect known for FGK stars. The errors in FWHM are  $\sim 0.3 \text{ km s}^{-1}$ , smaller than the size of the symbols.

of widths, the intrinsic line widths must have a lower limit of  $7.1 \text{ km s}^{-1}$  for K7-M5 dwarfs. There appear to be few, if any, stars from K7-M5 having lines narrower than  $7.1 \text{ km s}^{-1}$ , even among those fainter than  $M_V = 14$ . Such a lower limit to the Ca II H and K line widths would indicate a departure from the monotonic Wilson-Bappu relation set by the brighter M dwarfs. Perhaps some other broadening mechanism besides line transfer effects sets a floor on the FWHM of these lines. Spectra with very high resolution of a sample of M3-M8 dwarfs at Ca II H and K could verify this possible discontinuity or breakdown of the Wilson Bappu effect in M dwarfs.

The values plotted in Figure 5 are the means of multiple measurements from each star, and reveal considerable spread in FWHM at a given  $M_V$ . We examined the standard deviations of the multiple measurements for individual stars to determine if vertical spread in Figure 5 could be due to temporal changes in the stars. The maximum standard deviation for individual stars is  $\sim 0.76 \text{ km s}^{-1}$ , the same variance as the observed vertical spread among the different stars. But the typical standard deviation of  $0.35 \text{ km s}^{-1}$  is considerably less than the vertical spread in Figure 5. Thus the distribution in FWHM among stars at a given

mass is due in part to temporal variability, but the spread is dominated by the distribution of rotation and perhaps by the degeneracy of mass for a given  $M_V$ .

Close inspection of Figure 5 shows that the K lines are generally wider than the H lines. Figure 6 shows a histogram of the difference between the mean FWHM of the K line and that of the H line for each star. The distribution is displaced toward positive values by  $1.5 \text{ km s}^{-1}$ . This greater width of the K line undoubtedly results from the slight difference in the radiative transfer of the H and K emission lines.

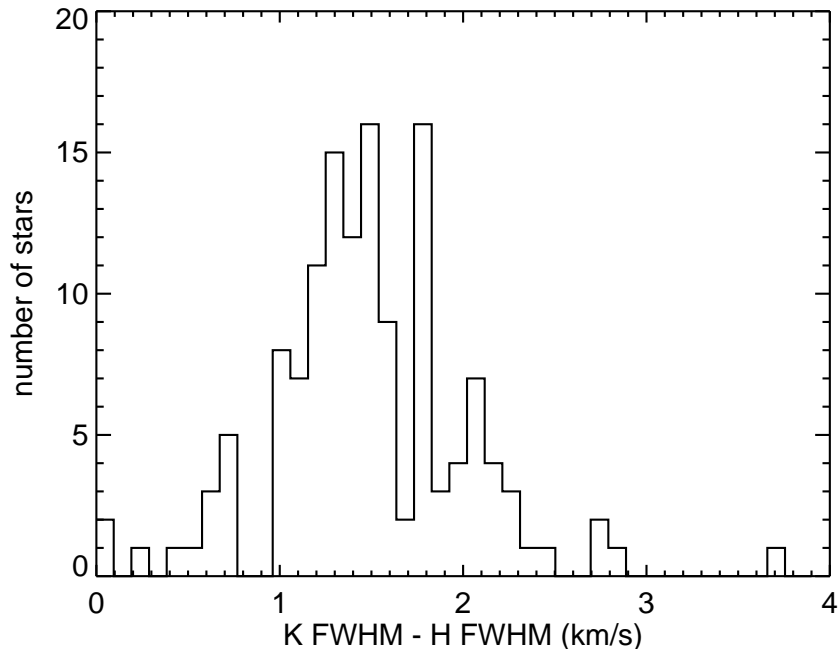


Fig. 6.— The distribution of the difference between average FWHM of the H and K emission lines. The K lines are systematically wider by  $1\text{-}2 \text{ km s}^{-1}$ .

The Ca II H and K emission lines arise from two upper states,  $^2P_{1/2}$  and  $^2P_{3/2}$ , respectively, and a common lower state,  $^2S$ . The different  $2J+1$  degeneracies of the two upper levels cause a slight enhancement of the source function of the K line over the H line at each height in the low density, upper chromosphere. In particular, radiative de-excitation of the K line occurs more commonly than for the H line. This difference causes the K line to approach the LTE emissivity limit (the Planck function) more closely than does the H line allowing the wings of the K line to grow faster, broadening its final profile. However, a full description of the differing widths of the H and K lines requires a detailed radiative transfer model, including the pressure, temperature, mass columns and velocity fields as a function of height in the chromosphere, along with the partial redistribution of photon frequencies during transitions.

## 4.2. Line asymmetry

Due to the high resolution of these spectra, many of the Ca II H and K line profiles are visibly asymmetric. Figure 7 shows representative spectra from three stars with asymmetry in the Ca II H line that is visible to the eye as a redshift of the central absorption (relative to the main emission). Our V/R and  $\Delta\lambda_c$  measurements permit quantitative analysis of this effect for lines with obvious asymmetry and more subtle cases.

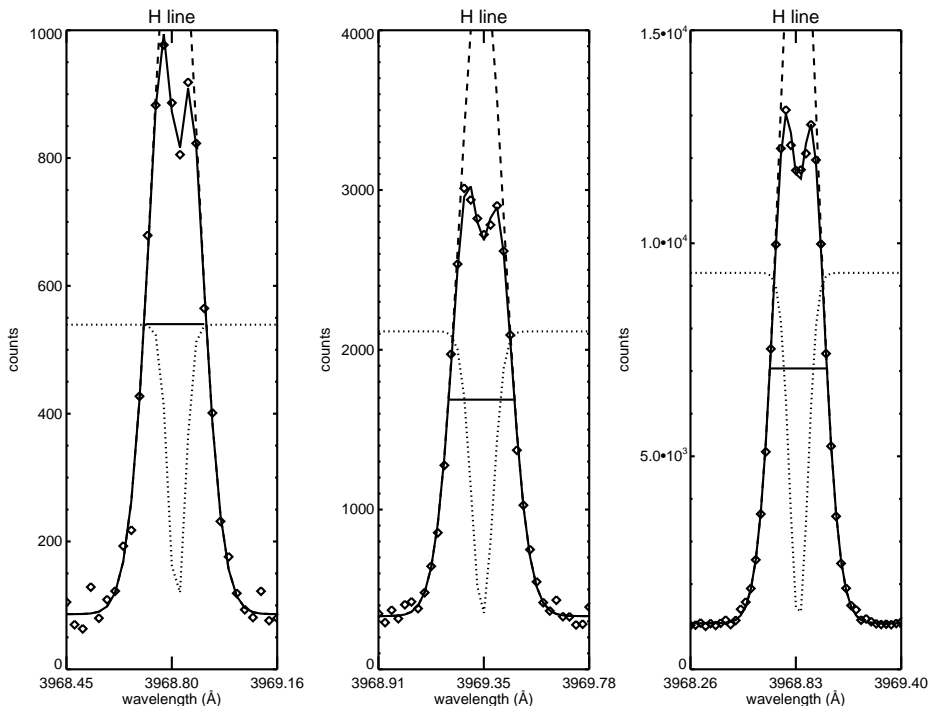


Fig. 7.— Representative Ca II H lines showing the data (dots), the model fits (solid line), and the component Gaussians (emission and absorption as dashed and dotted lines, respectively). Line asymmetry from central absorption redshifts of  $\Delta\lambda_c = 0.4, 0.2,$  and  $0.1 \text{ km s}^{-1}$  (left, middle, right) is clearly observable in the line profile data and model fits. The left spectrum is of GJ 413, middle spectrum of GJ 424, and right spectrum of GJ 338A.

In Figures 8 and 9 we plot V/R and  $\Delta\lambda_c$  versus  $M_V$ . The two figures show that there is little correlation between asymmetry and absolute magnitude. Figure 9 shows an increased spread in  $\Delta\lambda_c$  with higher  $M_V$ , i.e. for lower mass stars. This scatter is most likely due to the fact that these less luminous stars have noisier lines and therefore often have lower quality fits. Visual inspection of the spectra with  $|\Delta\lambda_c| > 2.5 \text{ km s}^{-1}$  confirms that these spectra tend to have a lower signal-to-noise ratio, and that the noise may be detrimentally affecting the fits. However, these plots clearly show that most stars have V/R greater than 1 and  $\Delta\lambda_c$  greater than 0, both indicating the presence of redshifted central absorption.

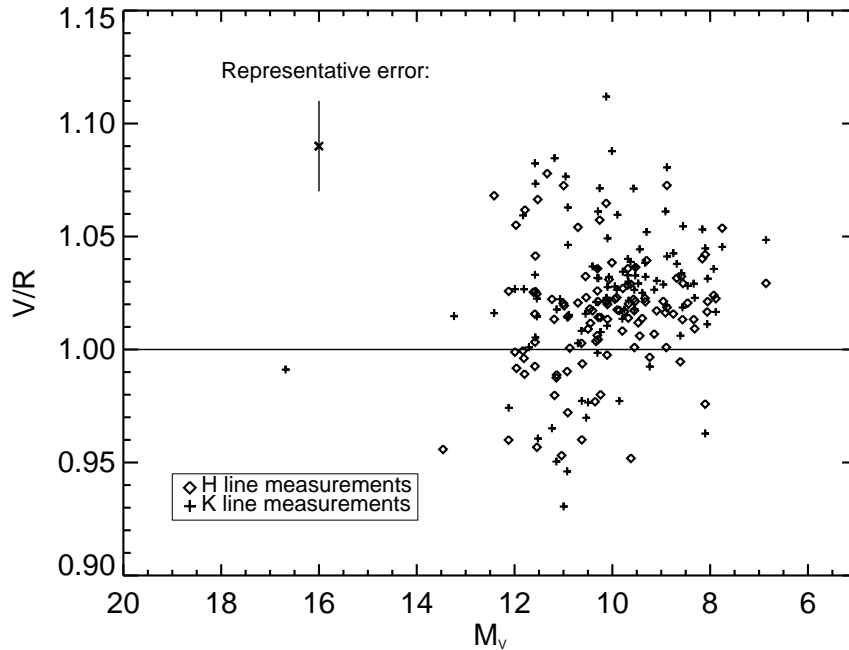


Fig. 8.— Asymmetry measure of Ca II H and K ,  $V/R$ , vs.  $M_V$ . The solid line represents no asymmetry, above which the domain represents lines having redshifted central absorption. Most K7-M5 dwarfs apparently have redshifted absorption reversals. Representative errors are shown for  $V/R$ .

As illustrated in the bottom plot of Figure 9, the central absorption redshifts for these stars tend to be  $\sim 0.1 \text{ km s}^{-1}$ . Such small redshifts may seem difficult to detect, but they correspond to 0.05 pixels, easily detectable with signal-to-noise ratios above 20, characteristic of these spectra. The measured redshifts for the representative Ca II H lines in Figure 7 are  $0.1\text{-}0.4 \text{ km s}^{-1}$  and clearly visible to the eye. The atmospheres of these stars must have gas with low source function that either has lower outward velocity or higher inward velocity than the higher source function gas below it. The relative speed of  $0.1 \text{ km s}^{-1}$  is remarkable both in its consistency among the M dwarfs and in its small magnitude. This speed is much slower than the escape velocity, indicating that the gas is not falling ballistically. Instead, it implies gas slowly decelerating upward or sinking downward slowly, with velocities controlled by gas pressure differences or magnetic forces.

Just as Figure 5 showed possible evidence of wider K lines than H lines, Figure 9 shows that the K line central absorption is typically more redshifted than the H line counterpart. To quantify this, we plot H line asymmetry measurements versus K line asymmetry measurements for each star in Figure 10.

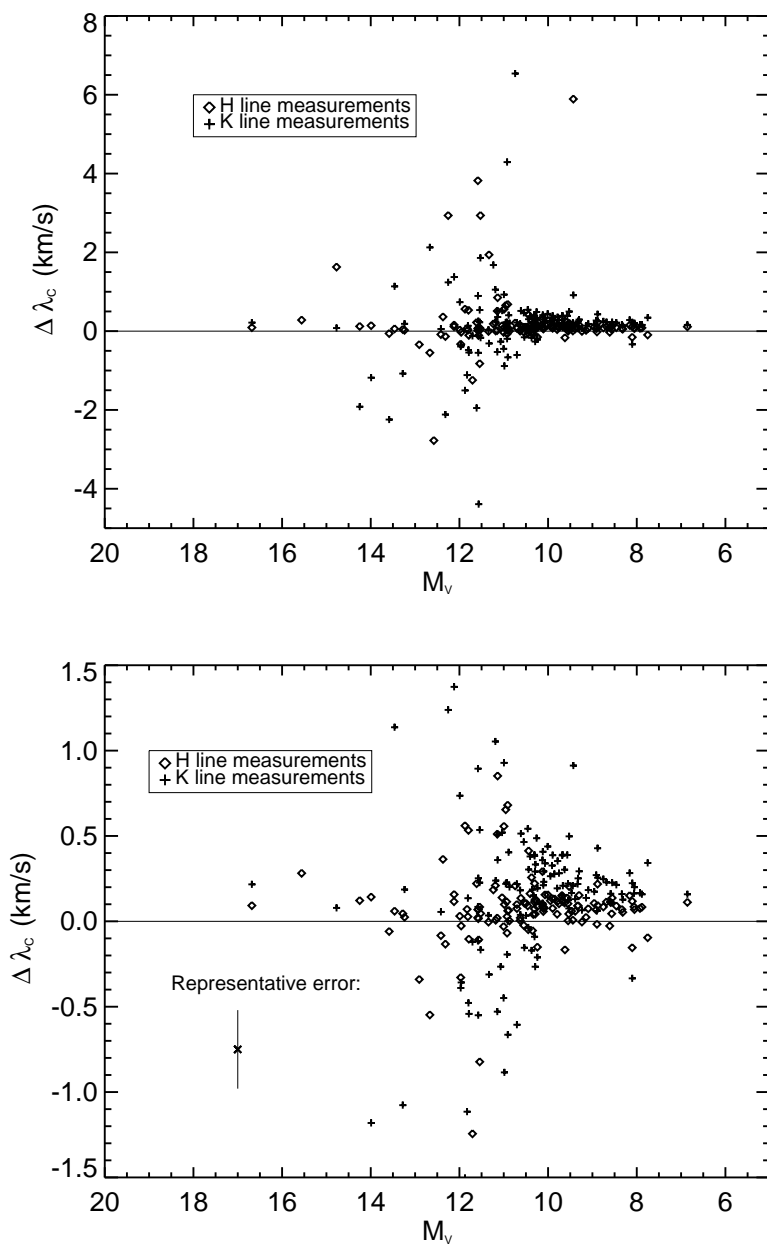


Fig. 9.— Redshift of the absorption reversal of Ca II H and K ,  $\Delta\lambda_c$ , vs.  $M_V$ . Top: the full range of values. Bottom: the domain within  $\pm 1.5$  km s $^{-1}$  of symmetry. The predominance of points *above* the horizontal line shows that most K7-M5 dwarfs have redshifted absorption reversals. Representative errors in the top plot are about the size of the plot symbols, and are shown in the bottom plot.

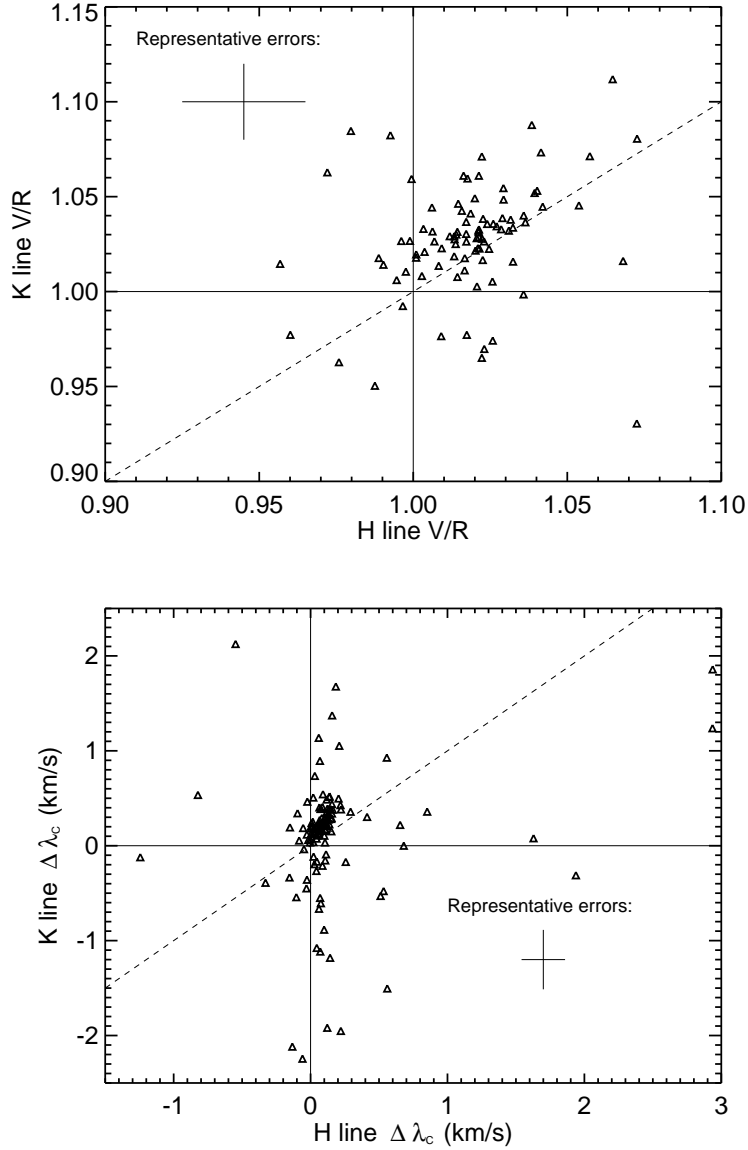


Fig. 10.— The correlation between asymmetry in the Ca II H and K lines measured two ways, using V/R (top) and  $\Delta\lambda_c$  (bottom). The solid lines separate measured redshifted absorption from blueshifted absorption. The dashed lines show an identity relation between the two variables. The asymmetries in the H and K lines are clearly correlated, albeit with scatter due to the measurement errors. The standard deviation of the residuals to a fit of the V/R data to the identity relation is 0.024, which is roughly equal to the V/R error. For the  $\Delta\lambda_c$  data, the standard deviation is  $0.7 \text{ km s}^{-1}$ , while the measurement error is  $\sim 0.23 \text{ km s}^{-1}$ .

If every star had an H line central absorption redshifted by the same amount as its K line central absorption, we would expect to see an identity relation in a plot of these parameters. Although our errors may be overestimated, visual inspection of Figure 10 shows an excess of points above the identity line, indicating a higher redshift for the absorption reversal of the K line. This implies that the K line central absorption forms in a region with slightly slower outward speeds (or greater inward speeds) than both the gas where the H absorption reversal forms and the gas where the H emission forms. This result is consistent with a progression of decreasing outward velocities, from lower to upper chromosphere.

Lastly, we find an interesting possible trend between the average asymmetry and EWs of the H and K lines. Figure 11 shows more scatter in the asymmetry of a line at EWs less than about 1 Å, while at EWs up to 2 Å the asymmetry tends to a smaller range of slightly redshifted values. Lines with low EWs may be weak and therefore more likely to have noise disrupt their fits, but visual inspection of these lines shows that this cannot account for all of the spread seen in Figure 11. This indicates a possible connection between the physics governing the chromospheric activity of a star and the velocity gradient in the chromosphere, such that as a star becomes more active its central absorption becomes redshifted.

### 4.3. Comparison with H $\alpha$ data

Here we compare the Ca II H and K equivalent widths to previously published H $\alpha$  equivalent widths taken from Gizis et al. (2002). H $\alpha$  equivalent widths have long been a standard measure of chromospheric heating in M dwarfs. By comparing the Ca II resonance lines to H $\alpha$  emission, the non-radiative heating and gas conditions in the lower and upper chromosphere may be compared.

H $\alpha$  has been extensively studied with regard to chromospheric and coronal heating in M dwarfs, indicating a peculiar behavior (Cram & Mullan 1979; Giampapa et al. 1982). With increasing magnetic fields, the Balmer lines first become stronger *in absorption* before they fill in and eventually go into emission. In contrast, the Ca II lines increase monotonically with increased magnetic heating (Cram & Mullan 1979). Due to this monotonic behavior, the Ca II emission strength provides a less ambiguous diagnostic of the magnetic state of the stellar surface than does H $\alpha$  (Doyle et al. 1994). Nonetheless, the most magnetically active M dwarfs, notably those with strong coronal emission, always show H $\alpha$  in emission. In Figure 12 we plot the H $\alpha$  equivalent width against the Ca II H and K equivalent width for our sample of M dwarfs. The H $\alpha$  equivalent width remains negative (absorption) near a value of about -0.2 Å for a wide range of Ca II EWs less than 2 Å. The H $\alpha$  absorption varies little with increasing Ca II H and K equivalent width up to 2 Å.

However, for Ca II H and K equivalent widths above  $\sim 2$  Å, H $\alpha$  abruptly goes into emission and increases monotonically with increasing Ca II H and K. The uncorrelated behavior between Ca II and H $\alpha$  for stars with H $\alpha$  in absorption has been seen before and attributed to highly segregated regions of line formation (Giampapa et al. 1989). Giampapa et al.

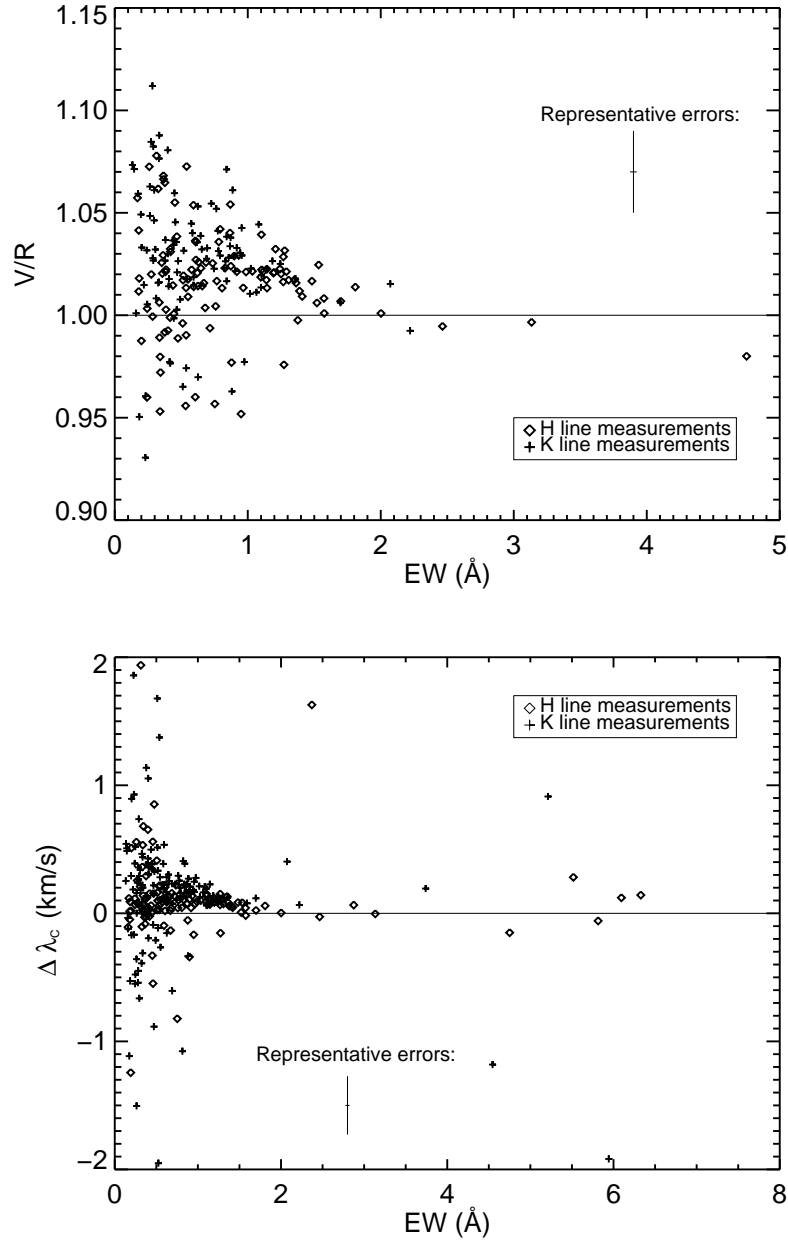


Fig. 11.— Asymmetry measurements versus Ca II H and K EW. The solid lines separate emission having redshifted from blueshifted central absorption. Most stars have a redshifted absorption reversal. The scatter in redshift is larger for stars with small EW, possibly a result of the larger measurement error in asymmetry associated with weaker emission. Representative errors are shown in both plots.

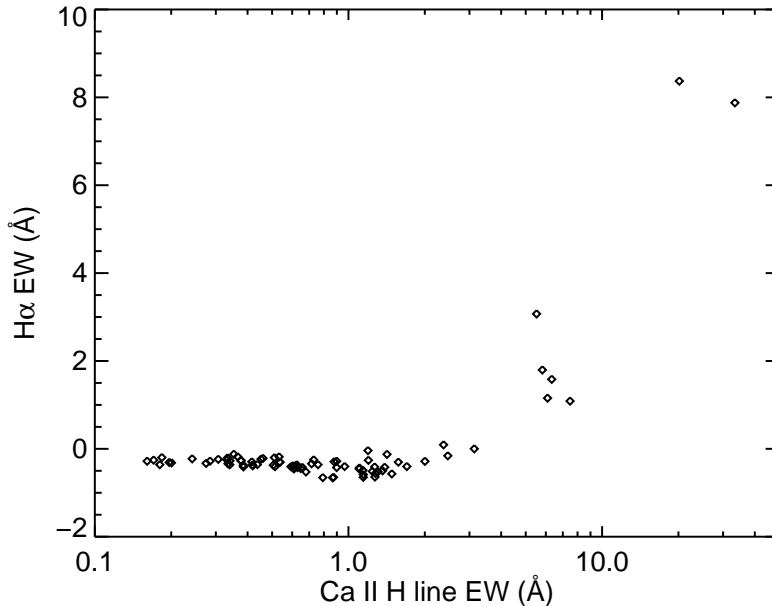


Fig. 12.— Ca II H line EWs versus previously published H $\alpha$  EWs for the same stars. The two emission lines are correlated only for large Ca II H and K emission above EW = 3 Å. This indicates that a magnetic threshold exists for H $\alpha$  while Ca II H and K remains a useful chromospheric diagnostic at all activity levels. H $\alpha$  EW values were taken from Gizis et al. (2002). Ca II EW errors are 0.025 Å.

(1982) found that the Ca II K line is formed in the lower chromosphere, while the H $\alpha$  line is formed in the upper chromosphere with a different cooling rate. The data presented here agree with such previously reported behavior and reflect this segregation. The suggestion is that the effect of magnetic fields on the two emitting regions remains separate until a certain level of magnetic heating is reached, at which point the lower and upper portions of the chromosphere behave similarly.

## 5. Discussion and Summary

The Ca II H and K line profiles of the 143 K7-M5 dwarfs examined here revealed various properties of their chromospheres and variations with stellar mass. The Ca II H and K line widths and fluxes increase with increasing stellar mass and luminosity, reminiscent of the Wilson-Bappu effect.

The latest type stars here ( $\sim$ M4-M5) have Ca II H and K emission line widths no more than 7.1 km s $^{-1}$  (FWHM), and possibly smaller as limited by our spectral resolution of 5.5

km s<sup>-1</sup>. In contrast, the higher mass M dwarfs have Ca II H and K emission line widths of 30 km s<sup>-1</sup>. Thus, the Ca II H and K line widths vary with stellar mass by a factor of  $\sim 4$  (from 7.1 to  $\sim 30$  km s<sup>-1</sup>) over the spectral type range from M5-K7, corresponding to a range of stellar mass from 0.3-0.55 M<sub>⊙</sub>. It is remarkable that the line widths vary roughly as the square of stellar mass. The broadening seen in the Ca II H and K lines is caused either by curve of growth effects in the line wings as the core approaches optical depth unity, or by broadening due to velocity fields (Eason et al. 1992). Apparently the structure of chromospheres changes significantly over this relatively small range in stellar mass.

The Ca II K line is consistently wider than the H line in all K7-M5 dwarfs, and its central absorption is consistently more redshifted (relative to the chromospheric emission). While the unequal degeneracies in the upper levels producing these lines cause somewhat differing optical depths, these data emphasize that the H and K lines are produced in slightly different regions of the chromosphere and are therefore governed by slightly different line transfer and kinematics.

Most of the K7-M5 stars exhibited redshifted central “absorption” reversals superimposed on the emission core, with an typical shift of 0.1 km s<sup>-1</sup>. As the absorption occurs at line center, that part of the line profile must form higher in the atmosphere near optical depth unity at line center. The redshifted “absorption” indicates that this higher material has a lower source function and that it is moving outward more slowly (or inward more quickly) than the lower material that has a higher source function.

The redshifted reversal can be explained with a simple heuristic model. Prominence-like or micro-flare activity results in chromospheric gas being magnetically heated and thrust outward. The outward moving, dense gas produces the Ca II emission while the material above it has expanded and cooled, and is moving more slowly. That upper material has lower density (and perhaps slightly lower temperature), yielding a lower source function. In such a picture, the gas decelerates after the initial outward kick. However, the observed 0.1 km s<sup>-1</sup> is much slower than free-fall, ballistic speeds. Thus, the modest velocity difference of 0.1 km s<sup>-1</sup> implies a fluid velocity gradient that is governed by magnetic fields or small gas pressure differences. These small and steady velocity gradients may be compared to the more violent kinematics that occur in major flares in M dwarfs (Hawley et al. 2003). Full NTLE models with kinematics will be constructed by Lucianne Walkowicz, in progress.

Stars with lower Ca II H and K equivalent widths exhibited a larger spread in the redshift of the absorption component. Between EWs of  $\sim 1$ – $2$  Å the redshift was confined to a small range near 0.1 km s<sup>-1</sup>; stars with weaker emission exhibited a wider range of redshifts. Thus there appears to be some relationship between the physical effects that govern the EW and the velocity fields.

The standard deviations from the mean values measured for both EWs and FWHMs were greater than our measurement errors, confirming that temporal changes do occur for these stars. Unfortunately, the degeneracy between  $M_V$  and stellar mass produces spread in our plots that cannot be distinguished from spread due to temporal variability or the influ-

ence of individual stellar parameters (e.g. age, rotation rate, metallicity) on chromospheric heating.

As previously found, there is clear evidence here of segregation between the region of the chromosphere that produces  $H\alpha$  and that which produces Ca II H and K for stars with  $H\alpha$  in absorption. However, at Ca II EWs greater than about  $2 \text{ \AA}$  we find a strong correlation between Ca II H and K and  $H\alpha$ . Apparently the upper and lower regions of chromospheres in M dwarfs behave independently until some magnetic activity threshold is reached, at which point they become governed by the same physical mechanism.

The results in this paper offer empirical suggestions of structural and kinematic attributes of M dwarf chromospheres that depend on stellar mass and vary with height. Models will be needed that include the non-LTE, partial redistribution line transfer of the Ca II H and K lines in atmospheres that contain velocity fields, to thoroughly explain the observed properties of chromospheric line profiles. In addition, stellar mass estimates are required to study the relation between chromospheric activity and mass. Finally, contemporaneous high resolution optical and UV spectra along with X-ray measurements would help constrain the relationship between chromospheres and coronae in M dwarfs.

We thank R. Paul Butler, Steve Vogt, and Jason Wright for obtaining most of the spectra used here. We thank Gibor Basri and Lucianne Walkowicz for valuable conversations. We appreciate many valuable comments provided by the anonymous referee, making the paper much richer. We acknowledge support from NASA grants NCC5-96 and NCC5-511 as well as NSF grant HRD-9706268. We wish to especially thank those of Hawaiian ancestry on whose sacred mountain of Mauna Kea we are privileged to be guests. Without their generous hospitality, the Keck observations presented herein would not have been possible.

Table 1. Observed stars

GJ	HIP	Other	Spectral type	$M_V$	B-V	Number of obs.	Begin (JD-2440000)	End (JD-2440000)
	428		M1	9.67	1.48	21	11757.10	12989.71
1	439	HD 225213	M1.5	10.37	1.46	3	12600.79	12899.00
14	1368		K7	8.06	1.42	10	12097.03	12924.89
15	1475	HD 1326	M1.5	10.31	1.56	25	10461.77	12924.89
15B		HD 1326B	M3.5	13.28	1.80	19	10667.00	13197.08
1009	1734		M1.5	9.86	1.48	4	12600.80	13196.06
26			M2.5	10.55	1.54	26	11581.71	12988.81
27	3143		M0.5	9.62	1.46	4	12600.80	13196.08
48	4856		M3	10.40	1.46	16	10667.04	13197.11
49	4872		M1.5	9.55	1.50	18	10667.05	13197.11
54.1	5643		M4.5	14.25	1.85	15	11012.05	13196.09
	8051		M2	10.70	1.52	10	11581.76	12926.06
83.1			M4.5	13.99	1.82	18	11411.04	12989.75
		G 244-047	M3	11.23	1.54	9	11581.79	12850.07
87	10279		M1.5	9.95	1.43	18	11410.13	13045.71
	11048		M0.5	8.96	1.51	18	11581.80	12897.96
105B			M4	12.37	1.62	2	12830.12	12988.77
109	12781		M3	11.19	1.55	13	11410.10	12854.11
156		SAO 130811	K7	8.10	1.37	19	10461.85	12897.99
	20917	HD 28343	K7	8.05	1.38	13	11226.80	12898.05
	21553	HD 232979	K7	8.59	1.43	10	11543.96	12898.04
	21556		M1.5	10.13	1.52	10	11580.78	12899.04
176	21932	HD 285968	K5	10.10	1.51	19	10839.76	12898.12
	22627		M3.5	11.54	1.60	14	11580.83	13016.83
180	22762		M2	10.44	1.52	7	11580.79	12898.10
	23512		M3	11.87	1.66	10	11543.90	12899.10
191	24186	HD 33793	M1	10.92	1.54	11	11170.92	12988.87
	24284		M2	10.29	1.55	6	12899.08	13045.74
205	25878	HD 36395	M1.5	9.14	1.52	19	10420.00	12924.99
		G 097-054	M3.5	11.34	1.59	6	11580.84	12899.11
208	26335	HD 245409	K7	8.61	1.44	21	10420.01	12899.12
	26801	HD 233153	M0.5	9.39	1.44	9	11580.77	12925.00
213	26857		M4	12.67	1.67	8	11550.89	12924.07
		G 192-013	M3.5	12.32	1.60	10	11543.99	12925.03
	29052		M4	11.58	1.60	8	11580.85	12988.93

Table 1—Continued

GJ	HIP	Other	Spectral type	$M_V$	B-V	Number of obs.	Begin (JD-2440000)	End (JD-2440000)
226	29277		M2	10.62	1.51	13	10839.95	12925.05
229	29295	HD 42581	M1	9.33	1.51	21	10420.06	12924.15
239	31635	HD 260655	K7	9.67	1.46	13	10839.94	12924.11
250B			M2	10.35	1.42	1	12924.09	12924.09
251	33226	HD 265866	M3	11.18	1.58	16	10784.07	12925.08
273	36208		M3.5	11.99	1.53	14	10805.89	12988.95
	36338		M3	10.99	1.42	6	11580.87	12988.96
	36834		M0.5	10.50	1.70	10	11580.89	13045.80
	37217		M3	11.52	2.00	6	11580.86	12925.13
285	37766		M4.5	12.25	1.61	9	11544.07	13076.97
2066	40501		M2	10.24	1.50	13	10805.88	13017.87
	41689		K7	8.88	1.35	5	12989.02	13077.03
	42220		K7	8.57	1.42	5	12989.03	13077.02
324		HD 75732B	M4	12.58	1.65	11	11544.12	12988.99
338A	45343	HD 79210	K7	8.68	1.43	18	10607.75	12989.04
338B	120005	HD 79211	K7	8.75	1.42	19	10607.76	12989.04
	46655		M3.5	11.80	1.60	14	11544.11	13017.88
	46769		M0	9.53	1.48	4	12989.06	13077.04
357	47103		M2.5	11.14	1.57	13	10839.97	12989.11
	47513		M1.5	10.12	1.50	10	11580.94	13017.97
	47650		M3	10.89	1.80	8	11580.91	12989.08
	48714		M0	8.90	1.47	13	11552.03	13017.94
382	49986	SAO 137411	M1.5	9.80	1.51	20	10607.76	13017.96
388		SAO 81292	M3.5	11.07	1.54	11	12064.85	13044.88
390	51007		M1	9.69	1.45	12	11580.98	13045.88
393	51317		M2	10.33	1.52	19	10607.77	13045.86
394		HD 237903	K7	8.56	1.34	2	12804.82	13044.89
	51468	HD 90875	K5	6.86	1.18	13	11200.05	13044.90
397	51525		K5	7.88	1.33	18	11200.06	13044.90
402	53020		M4	12.91	1.68	10	11552.11	13017.99
406			M5.5	16.68	2.00	16	11172.07	13018.00
408	53767		M2.5	10.92	1.55	18	10607.79	13077.05
410	53985	HD 95650	M0	9.24	1.44	18	11581.03	13077.05
411	54035	HD 95735	M2	10.46	1.51	36	10602.91	13018.16
412A	54211	SAO 43609	M0.5	10.26	1.54	19	10605.79	13077.08

Table 1—Continued

GJ	HIP	Other	Spectral type	$M_V$	B-V	Number of obs.	Begin (JD-2440000)	End (JD-2440000)
413	54532		M2	10.31	1.55	11	11552.09	13017.17
414B		HD 97101B	M1.5	9.57	1.57	6	12064.77	13044.98
414A	54646	HD 97101	K8	7.93	1.36	21	10463.01	13044.98
424	55360	SAO 15475	M0	9.53	1.42	10	11552.06	13018.15
433	56528	SAO 202602	M1.5	10.01	1.49	11	11200.04	13018.04
	57050		M4	11.79	1.60	10	11581.04	13077.10
436	57087		M2.5	10.63	1.52	78	11552.07	13196.77
445	57544		M3.5	12.12	1.59	15	10840.15	13018.11
447	57548		M4	13.46	1.77	14	10983.75	13018.03
450	57802	SAO 43609	M1	10.12	1.52	17	10840.13	13018.11
	59406	L 758-107	M4	12.08	1.40	11	11581.11	13018.06
465	60559		M4	11.57	1.62	13	11552.13	13018.08
486	62452		M3.5	11.83	1.56	19	10839.14	13046.07
	62687	HD 111631	K7	8.32	1.42	13	11582.07	13046.04
494A	63510		M0.5	9.43	1.45	22	11582.07	13046.05
514			M0.5	9.63	1.50	26	10546.01	13196.82
	66459	SAO 63647	K5	8.88	1.40	11	11581.07	13071.99
526	67155	HD 119850	M1.5	9.79	1.45	19	10546.02	13071.96
	67164		M3.5	11.53	1.54	13	11582.05	13179.80
	68469	HD 122303	M1	9.68	1.49	12	11410.73	13071.95
	70865		M2	9.90	1.47	5	12897.72	13179.79
	70975		M3.5	11.71	1.61	13	11582.09	13153.87
555	71253		M4	12.42	1.62	16	11410.73	13153.87
9492	71898	SAO 17568	M3	10.91	1.62	17	10840.16	13077.11
569A	72944		M2.5	10.24	1.48	12	12062.87	13153.93
581	74995		M3	11.57	1.61	15	11409.76	13077.15
	79755	HD 147379A	K7	8.46	1.41	16	11679.96	13179.94
		HD 147379B	M3	10.54	1.51	15	11679.97	13179.94
623	80346		M3	10.74	1.48	2	12062.92	12099.83
625	80459		M1.5	11.04	1.59	17	10862.14	13179.92
628	80824		M3.5	11.97	1.60	21	11409.75	13153.92
638	82003	HD 151288	K5	8.16	1.37	24	10601.99	13179.97
649	83043		M1	9.55	1.59	27	11409.82	13195.81
	83762		M3	10.95	1.56	3	12897.79	13181.93
	84099		M3.5	11.14	1.50	16	11678.94	13074.09

Table 1—Continued

GJ	HIP	Other	Spectral type	$M_V$	B-V	Number of obs.	Begin (JD-2440000)	End (JD-2440000)
667C			M1.5	11.00	1.57	14	11704.98	13153.97
	84790		M2.5	10.91	1.56	18	11704.94	13181.92
673	85295	HD 157881	K5	8.10	1.36	21	10275.88	13153.98
678	85665	SAO 122446	M0	9.32	1.45	18	10955.06	13153.98
687	86162	SAO 17568	M3	10.87	1.50	27	10603.96	13179.98
686	86287		M1	10.07	1.53	20	10604.94	13181.85
694	86776		M2.5	10.61	1.55	20	10956.10	13179.99
2130A	86961		M2	11.54	1.46	13	11702.95	13153.99
699	87937		M4	13.24	1.74	74	10602.00	13195.82
701	88574	HD 165222	M1	9.91	1.52	29	10602.02	13072.12
		LHS 462	M3	11.58	1.58	14	11704.96	13180.01
		G 205-028	M3.5	11.61	2.01	12	11705.98	13180.02
4063			M3.5	12.12	1.42	16	11409.86	13180.03
	91699		M3	11.00	1.63	15	11706.00	13181.91
725A	91768	HD 173739	M3	11.15	1.54	23	10602.05	13179.88
725B	91772	HD 173740	M3.5	11.96	1.59	21	10602.06	13179.97
729	92403		M3.5	13.58	1.60	25	10984.03	13154.00
745A	93873		M1.5	11.07	1.55	13	10982.94	13180.07
745B	93899	HD 349726	M1.5	11.01	1.55	14	10983.00	13180.06
		G 207-019	M3	11.33	1.80	12	11706.04	13180.05
752A	94761	HD 180617	M2.5	10.29	1.50	35	12061.95	13196.85
1245B			M5.5	15.56	1.98	3	12804.00	13154.10
	99427	HD 193202	K5	7.75	1.32	14	11342.00	13181.97
793	101180		M2.5	10.94	1.56	15	10983.98	13181.98
806	102401		M1.5	10.31	1.49	18	10602.10	13182.00
809	103096		M0.5	9.30	1.49	20	10602.11	13182.02
	104432		M1	10.45	1.49	13	11704.05	13182.05
846	108782	HD 209290	M0	9.09	1.46	18	11410.00	13196.92
849	109388		M3.5	10.70	1.52	22	11410.01	13196.93
	109555		M2	10.11	1.52	10	12095.09	13195.90
860A	110893	HD 239960	M3	11.58	1.65	20	10606.07	13180.98
873	112460		M3.5	11.77	1.54	19	12094.98	13196.95
876	113020		M4	11.81	1.60	144	10602.09	13196.99
880	113296	HD 216899	M1.5	9.47	1.51	22	10666.04	13195.96
884	113576	HD 217357	K5	8.34	1.39	41	10365.88	13197.01

Table 1—Continued

GJ	HIP	Other	Spectral type	$M_V$	B-V	Number of obs.	Begin (JD-2440000)	End (JD-2440000)
887	114046	HD 217987	M0.5	9.75	1.48	34	10984.12	13197.01
891	114411		M2	10.29	1.57	4	12600.73	13197.00
	115332		M4	11.58	1.50	12	11899.78	13197.02
	115562		M1	9.44	1.47	3	12897.87	12988.80
905			M5	14.77	1.91	16	11010.01	13197.06
908	117473	SAO 128397	M1	10.10	1.48	28	10366.88	13196.01
911	117886		K7	8.91	1.42	4	12600.78	13197.04

Table 2. Average H line parameters

GJ	HIP	Other	# good spectra <sup>a</sup>	EW (Å)	$\sigma_{EW}$ (Å)	FWHM (km s <sup>-1</sup> )	$\sigma_{FWHM}$ (km s <sup>-1</sup> )	$\Delta\lambda_c$ (km s <sup>-1</sup> )	$\sigma_{\Delta\lambda_c}$ (km s <sup>-1</sup> )	V/R	$\sigma_{V/R}$
	428		20	1.25	0.13	19.49	0.31	0.12	0.08	1.020	0.019
1	439	HD 225213	3	0.27	0.06	12.66	0.30	0.26	0.14	–	–
14	1368		10	1.48	0.10	23.82	0.25	0.09	0.07	1.017	0.018
15	1475	HD 1326	22	0.33	0.07	14.42	0.36	0.07	0.07	1.006	0.021
15B		HD 1326B	10	1.42	1.04	10.17	0.98	0.05	0.25	–	–
1009	1734		3	1.35	0.09	19.34	0.28	0.13	0.07	1.017	0.029
26			25	0.42	0.09	14.20	0.51	-0.02	0.24	1.032	0.034
27	3143		3	0.95	0.15	20.01	0.53	-0.17	0.23	0.952	0.096
48	4856		14	0.51	0.05	15.12	0.44	0.16	0.17	1.017	0.029
49	4872		18	2.00	0.24	19.92	0.28	0.00	0.05	1.001	0.011
54.1	5643		11	6.10	3.05	10.49	0.42	0.12	0.48	–	–
	8051		10	0.87	0.22	12.95	0.41	0.08	0.39	1.054	0.074
83.1			9	6.33	1.45	10.85	0.32	0.14	0.59	–	–
		G 244-047	7	0.58	0.08	15.32	0.25	0.18	0.15	1.022	0.132
87	10279		17	0.39	0.05	16.80	0.44	0.12	0.14	1.022	0.041
	11048		18	1.29	0.15	22.06	0.50	0.11	0.07	1.021	0.019
105B			1	0.33	–	10.26	–	0.36	–	–	–
109	12781		10	0.54	0.11	11.75	0.38	0.21	0.35	1.013	0.005
156		SAO 130811	19	0.79	0.08	25.67	0.48	0.12	0.07	1.042	0.028
	20917	HD 28343	13	1.11	0.12	24.94	0.70	0.07	0.08	1.021	0.020
	21553	HD 232979	10	1.21	0.05	22.88	0.36	0.11	0.05	1.032	0.018
	21556		10	0.38	0.04	17.78	0.50	0.29	0.23	1.065	0.072
176	21932	HD 285968	19	0.97	0.10	17.23	0.40	0.07	0.08	1.013	0.026
	22627		12	0.75	0.08	11.51	0.40	-0.82	2.78	0.957	0.063
180	22762		7	0.51	0.13	12.70	0.49	0.41	0.54	–	–
	23512		3	0.46	0.07	9.92	0.30	0.56	0.23	–	–

Table 2—Continued

GJ	HIP	Other	# good spectra <sup>a</sup>	EW (Å)	$\sigma_{EW}$ (Å)	FWHM (km s <sup>-1</sup> )	$\sigma_{FWHM}$ (km s <sup>-1</sup> )	$\Delta\lambda_c$ (km s <sup>-1</sup> )	$\sigma_{\Delta\lambda_c}$ (km s <sup>-1</sup> )	V/R	$\sigma_{V/R}$
191	24186	HD 33793	3	–	–	10.86	0.80	-0.07	2.79	–	–
	24284		6	0.38	0.03	15.76	0.42	0.12	0.06	1.021	0.022
205	25878	HD 36395	18	1.70	0.12	21.70	0.33	0.02	0.05	1.007	0.012
		G 097-054	4	0.38	0.03	11.15	0.63	0.00	0.22	–	–
208	26335	HD 245409	15	2.46	0.13	21.40	0.31	-0.03	0.13	0.995	0.014
	26801	HD 233153	9	1.81	0.19	21.06	0.36	0.06	0.08	1.014	0.019
213	26857		5	0.46	0.21	9.82	0.44	-0.55	0.88	–	–
		G 192-013	8	0.67	0.15	10.21	0.51	-0.13	0.72	–	–
	29052		3	0.40	0.16	10.61	0.78	3.82	4.02	0.993	–
226	29277		5	0.61	0.10	13.65	0.46	0.02	0.48	0.960	–
229	29295	HD 42581	21	1.24	0.14	21.10	0.43	0.09	0.05	1.023	0.015
239	31635	HD 260655	13	0.59	0.09	17.65	0.45	0.12	0.09	1.014	0.019
250B			1	0.88	–	15.43	–	-0.05	–	0.977	–
251	33226	HD 265866	14	0.34	0.06	11.66	0.42	0.01	0.19	0.980	0.034
273	36208		12	0.42	0.11	10.69	0.31	0.03	0.08	0.999	0.052
	36338		5	0.52	0.17	12.02	0.60	0.10	0.56	1.019	–
	36834		10	0.55	0.06	14.20	0.43	0.11	0.15	1.009	–
	37217		1	0.40	–	11.31	–	0.05	–	–	–
285	37766		1	20.16	–	15.89	–	2.94	–	–	–
2066	40501		12	0.63	0.09	14.90	0.34	0.09	0.10	1.014	0.030
	41689		3	0.54	0.04	22.97	0.33	0.22	0.12	1.073	0.057
	42220		5	0.81	0.05	23.83	0.30	0.04	0.14	1.013	0.039
324B		HD 75732B	1	0.73	–	9.23	–	-2.78	–	–	–
338A	45343	HD 79210	16	1.28	0.11	23.04	0.41	0.11	0.05	1.032	0.014
338B	120005	HD 79211	19	1.36	0.09	22.72	0.33	0.08	0.05	1.016	0.009
	46655		8	0.34	0.05	10.39	0.82	0.53	0.81	0.989	–

Table 2—Continued

GJ	HIP	Other	# good spectra <sup>a</sup>	EW (Å)	$\sigma_{EW}$ (Å)	FWHM (km s <sup>-1</sup> )	$\sigma_{FWHM}$ (km s <sup>-1</sup> )	$\Delta\lambda_c$ (km s <sup>-1</sup> )	$\sigma_{\Delta\lambda_c}$ (km s <sup>-1</sup> )	V/R	$\sigma_{V/R}$
	46769		4	0.92	0.07	20.02	0.41	0.04	0.11	1.021	0.013
357	47103		6	0.20	0.04	10.71	0.51	0.51	2.97	0.988	0.103
	47513		10	1.03	0.13	17.30	0.35	0.10	0.16	1.022	0.030
	47650		7	2.87	0.43	13.79	0.20	0.06	0.17	—	—
	48714		13	1.58	0.09	22.20	0.31	-0.02	0.08	1.001	0.015
382	49986	SAO 137411	20	1.57	0.13	18.69	0.31	0.04	0.05	1.008	0.010
388		SAO 81292	0	—	—	—	—	—	—	—	—
390	51007		11	1.27	0.12	19.88	0.40	0.15	0.11	1.029	0.027
393	51317		19	0.68	0.08	14.51	0.34	0.04	0.08	1.004	0.014
394		HD 237903	2	0.93	0.01	24.63	0.01	0.14	0.02	1.029	0.017
	51468	HD 90875	11	0.36	0.04	30.00	0.48	0.11	0.07	1.029	0.018
397	51525		18	1.14	0.09	24.60	0.62	0.08	0.16	1.023	0.027
402	53020		6	0.90	0.15	10.18	0.50	-0.34	0.71	—	—
406			4	33.39	14.65	11.56	0.29	0.09	0.20	—	—
408	53767		17	0.54	0.08	12.24	0.27	0.03	0.12	0.990	0.014
410	53985	HD 95650	11	3.13	0.33	20.31	0.35	0.00	0.08	0.997	0.011
411	54035	HD 95735	32	0.18	0.03	13.32	0.28	0.09	0.13	1.018	0.022
412A	54211	SAO 43609	10	0.17	0.03	14.40	0.45	0.12	0.07	1.057	0.037
413	54532		10	0.61	0.06	15.93	0.55	0.22	0.25	1.036	0.036
414B		HD 97101B	6	1.10	0.07	21.06	0.46	0.14	0.22	1.022	0.020
414A	54646	HD 97101	20	0.87	0.09	25.17	0.40	0.08	0.07	1.024	0.020
424	55360	SAO 15475	10	0.61	0.08	19.52	0.50	0.20	0.10	1.036	0.021
433	56528	SAO 202602	10	0.47	0.05	18.01	0.50	0.16	0.16	1.038	0.057
	57050		4	0.33	0.05	10.54	0.67	-0.10	1.00	1.062	0.021
436	57087		67	0.38	0.03	14.64	0.46	0.00	0.67	1.003	0.034
445	57544		8	0.24	0.07	9.98	0.73	0.12	1.05	0.960	0.065

Table 2—Continued

GJ	HIP	Other	# good spectra <sup>a</sup>	EW (Å)	$\sigma_{EW}$ (Å)	FWHM (km s <sup>-1</sup> )	$\sigma_{FWHM}$ (km s <sup>-1</sup> )	$\Delta\lambda_c$ (km s <sup>-1</sup> )	$\sigma_{\Delta\lambda_c}$ (km s <sup>-1</sup> )	V/R	$\sigma_{V/R}$
447	57548		10	0.53	0.19	9.76	0.42	0.06	0.18	0.956	–
450	57802	SAO 43609	17	1.20	0.12	16.82	0.34	0.09	0.13	1.021	0.015
	59406B	L 758-107	0	–	–	–	–	–	–	–	–
465	60559		1	0.16	–	10.26	–	-0.11	–	–	–
486	62452		12	0.28	0.04	10.65	0.55	0.07	0.55	0.999	0.082
	62687	HD 111631	13	1.41	0.12	23.31	0.34	0.05	0.07	1.009	0.020
494A	63510		2	7.48	0.17	22.08	0.00	5.89	0.82	–	–
514			26	0.90	0.08	19.34	0.28	0.11	0.06	1.029	0.016
	66459	SAO 63647	11	1.10	0.07	22.19	0.39	0.09	0.06	1.019	0.013
526	67155	HD 119850	18	0.61	0.09	18.04	0.44	0.12	0.04	1.027	0.019
	67164		3	0.37	0.07	10.94	0.31	2.94	5.14	1.066	–
	68469	HD 122303	11	0.78	0.09	19.58	0.36	0.15	0.06	1.036	0.019
	70865		5	0.55	0.07	19.31	0.45	0.08	0.02	1.018	0.019
	70975		2	0.19	0.04	11.03	0.38	-1.24	1.97	–	–
555	71253		10	0.37	0.05	10.83	0.29	-0.08	0.27	1.068	0.057
9492	71898	SAO 17568	13	0.44	0.11	12.39	0.51	0.06	0.50	1.015	0.052
569A	72944		1	4.75	–	16.43	–	-0.15	–	0.980	–
581	74995		12	0.18	0.02	11.13	0.71	0.02	0.28	1.041	0.032
	79755	HD 147379A	16	1.19	0.07	24.38	0.26	0.09	0.06	1.021	0.015
		HD 147379B	14	0.83	0.06	15.48	0.40	0.11	0.13	1.023	0.023
623	80346		2	0.31	0.07	11.06	0.37	0.21	0.47	–	–
625	80459		16	0.34	0.09	10.69	0.47	0.14	0.41	0.953	–
628	80824		16	0.45	0.10	10.59	0.41	-0.33	1.55	1.055	–
638	82003	HD 151288	24	0.87	0.07	24.62	0.26	0.15	0.04	1.040	0.016
649	83043		27	1.14	0.08	19.66	0.37	0.10	0.07	1.017	0.017
	83762		2	0.40	0.03	12.35	0.03	0.65	0.40	–	–

Table 2—Continued

GJ	HIP	Other	# good spectra <sup>a</sup>	EW (Å)	$\sigma_{EW}$ (Å)	FWHM (km s <sup>-1</sup> )	$\sigma_{FWHM}$ (km s <sup>-1</sup> )	$\Delta\lambda_c$ (km s <sup>-1</sup> )	$\sigma_{\Delta\lambda_c}$ (km s <sup>-1</sup> )	V/R	$\sigma_{V/R}$
	84099		12	0.48	0.07	12.30	0.41	0.85	2.66	0.989	–
667C			9	0.36	0.05	11.30	0.36	-0.03	0.65	1.020	–
	84790		9	0.34	0.04	11.42	0.50	0.68	2.92	0.972	0.021
673	85295	HD 157881	21	1.27	0.10	23.67	0.53	-0.15	0.08	0.976	0.014
678	85665	SAO 122446	17	0.99	0.13	20.22	0.40	0.09	0.07	1.021	0.026
687	86162	SAO 17568	26	0.44	0.08	12.36	0.57	0.00	0.13	1.001	0.030
686	86287		20	0.42	0.06	16.64	0.34	0.16	0.08	1.031	0.024
694	86776		18	0.72	0.13	14.25	0.39	0.14	0.17	0.994	0.017
2130A	86961		10	1.53	0.16	19.32	0.26	0.08	0.16	1.025	0.028
699	87937		51	0.33	0.11	9.11	0.35	0.02	0.20	–	–
701	88574	HD 165222	29	0.65	0.04	17.57	0.33	0.13	0.08	1.023	0.025
		LHS 462	3	0.24	0.04	10.27	0.52	0.07	0.15	1.003	–
		G 205-028	6	0.74	0.21	11.74	0.39	0.22	0.45	1.025	–
4063			14	0.69	0.10	14.23	0.59	0.16	0.31	1.026	0.064
	91699		12	0.26	0.09	11.99	0.71	0.56	2.97	1.073	0.050
725A	91768	HD 173739	19	0.20	0.05	10.81	0.36	0.02	0.16	–	–
725B	91772	HD 173740	13	0.38	0.14	9.88	0.38	-0.03	0.19	0.992	–
729	92403		10	5.82	1.24	11.35	0.44	-0.06	2.37	–	–
745A	93873		0	–	–	–	–	–	–	–	–
745B	93899	HD 349726	0	–	–	–	–	–	–	–	–
		G 207-019	4	0.31	0.10	10.15	0.51	1.94	1.42	1.078	–
752A	94761	HD 180617	35	0.66	0.06	17.19	0.29	0.13	0.07	1.014	0.015
1245B			1	5.52	–	14.38	–	0.28	–	–	–
	99427	HD 193202	14	0.59	0.14	25.58	5.75	-0.10	0.94	1.054	0.022
793	101180		12	1.19	0.12	11.85	0.46	0.11	0.24	–	–
806	102401		17	0.63	0.08	14.66	0.45	0.11	0.21	1.026	0.049

Table 2—Continued

GJ	HIP	Other	# good spectra <sup>a</sup>	EW (Å)	$\sigma_{EW}$ (Å)	FWHM (km s <sup>-1</sup> )	$\sigma_{FWHM}$ (km s <sup>-1</sup> )	$\Delta\lambda_c$ (km s <sup>-1</sup> )	$\sigma_{\Delta\lambda_c}$ (km s <sup>-1</sup> )	V/R	$\sigma_{V/R}$
809	103096		20	1.10	0.09	21.66	0.30	0.15	0.04	1.039	0.014
	104432		10	0.18	0.02	11.48	0.59	-0.05	0.59	1.012	0.096
846	108782	HD 209290	18	1.31	0.12	21.75	0.47	0.07	0.05	1.017	0.014
849	109388		21	0.62	0.04	16.35	0.42	0.10	0.13	1.021	0.026
	109555		9	1.38	0.17	18.98	0.41	0.06	0.08	0.998	0.016
860A	110893	HD 239960	15	0.35	0.07	10.63	0.42	0.07	0.12	1.026	0.032
873	112460		0	–	–	–	–	–	–	–	–
876	113020		132	0.51	0.11	11.44	0.39	0.03	0.24	0.996	0.027
880	113296	HD 216899	22	1.39	0.14	20.33	0.35	0.06	0.05	1.012	0.011
884	113576	HD 217357	40	1.14	0.08	23.29	0.33	0.07	0.06	1.013	0.015
887	114046	HD 217987	34	0.77	0.13	18.00	0.44	0.10	0.06	1.017	0.017
891	114411		4	0.76	0.08	14.65	0.51	0.04	0.28	1.004	–
	115332		11	0.67	0.13	11.40	0.39	0.02	0.41	1.016	–
	115562		3	1.52	0.19	20.57	0.51	0.01	0.03	1.006	0.005
905			9	2.37	1.07	9.44	0.37	1.63	3.31	–	–
908	117473	SAO 128397	28	0.27	0.04	14.12	0.43	0.08	0.10	1.020	0.018
911	117886		4	1.27	0.08	22.08	0.42	0.07	0.21	1.016	0.050

<sup>a</sup>Occasionally our automated process could not fit the line(s) in a spectrum, or the fit was of bad quality and had to be rejected. This column lists the number of spectra in which the H line was successfully fit for each star.

Table 3. Average K line parameters

GJ	HIP	Other	# good spectra <sup>a</sup>	EW (Å)	$\sigma_{EW}$ (Å)	FWHM (km s <sup>-1</sup> )	$\sigma_{FWHM}$ (km s <sup>-1</sup> )	$\Delta\lambda_c$ (km s <sup>-1</sup> )	$\sigma_{\Delta\lambda_c}$ (km s <sup>-1</sup> )	V/R	$\sigma_{V/R}$
	428		20	0.91	0.10	20.83	0.58	0.21	0.21	1.022	0.031
1	439	HD 225213	3	0.20	0.04	13.84	0.01	-0.17	0.25	–	–
14	1368		10	1.07	0.07	25.71	0.47	0.16	0.16	1.011	0.019
15	1475	HD 1326	24	0.24	0.04	15.42	0.45	0.39	0.35	1.032	–
15B		HD 1326B	8	0.81	0.54	10.04	0.86	-1.07	1.45	–	–
1009	1734		4	0.97	0.07	21.04	0.44	0.27	0.49	0.977	0.005
26			21	0.33	0.06	15.33	0.77	0.46	1.17	1.016	0.016
27	3143		0	–	–	–	–	–	–	–	–
48	4856		12	0.38	0.04	16.44	0.36	0.38	0.53	1.037	0.053
49	4872		18	1.36	0.15	21.24	0.27	0.12	0.15	1.018	0.017
54.1	5643		6	5.94	3.92	11.07	0.35	-1.90	0.93	–	–
	8051		7	0.69	0.17	14.01	0.53	-0.60	0.76	–	–
83.1			5	4.54	0.74	11.76	0.24	-1.17	2.79	–	–
		G 244-047	2	0.51	0.03	16.94	0.35	1.66	2.07	0.965	–
87	10279		16	0.29	0.04	17.97	0.64	0.26	0.53	1.028	0.039
	11048		18	0.90	0.10	23.63	0.58	0.17	0.09	1.029	0.017
105B			0	–	–	–	–	–	–	–	–
109	12781		8	0.40	0.08	12.87	0.58	1.04	2.43	–	–
156		SAO 130811	18	0.58	0.04	27.75	0.63	0.22	0.16	1.045	0.038
	20917	HD 28343	13	0.78	0.09	26.83	0.82	0.20	0.09	1.031	0.015
	21553	HD 232979	10	0.87	0.05	24.52	0.26	0.16	0.09	1.034	0.013
	21556		8	0.28	0.04	19.26	0.65	0.36	0.17	1.112	0.043
176	21932	HD 285968	19	0.69	0.08	18.44	0.41	0.23	0.32	1.028	0.021
	22627		6	0.59	0.06	12.75	0.69	0.53	2.70	1.015	–
180	22762		6	0.41	0.08	13.85	0.50	0.30	1.54	–	–
	23512		1	0.26	–	10.52	–	-1.49	–	–	–

Table 3—Continued

GJ	HIP	Other	# good spectra <sup>a</sup>	EW (Å)	$\sigma_{EW}$ (Å)	FWHM (km s <sup>-1</sup> )	$\sigma_{FWHM}$ (km s <sup>-1</sup> )	$\Delta\lambda_c$ (km s <sup>-1</sup> )	$\sigma_{\Delta\lambda_c}$ (km s <sup>-1</sup> )	V/R	$\sigma_{V/R}$
191	24186	HD 33793	3	–	–	12.28	0.84	4.25	6.25	0.946	–
	24284		6	0.30	0.04	17.37	0.45	0.29	0.17	1.061	0.078
205	25878	HD 36395	18	1.19	0.09	23.45	0.46	0.14	0.10	1.026	0.012
		G 097-054	2	0.33	0.02	12.46	0.39	0.03	0.48	–	–
208	26335	HD 245-409	15	1.70	0.10	22.99	0.29	0.12	0.13	1.006	0.015
	26801	HD 233153	8	1.24	0.17	22.44	0.41	0.13	0.10	1.025	0.020
213	26857		4	0.26	0.27	10.23	0.55	2.11	3.88	–	–
		G 192-013	3	0.52	0.03	11.26	0.30	-2.10	4.24	–	–
	29052		1	0.29	–	10.52	–	0.08	–	1.082	–
226	29277		5	0.41	0.08	13.74	0.60	0.04	1.45	0.977	0.026
229	29295	HD 42581	19	0.84	0.10	22.65	0.48	0.22	0.15	1.038	0.022
239	31635	HD 260655	13	0.40	0.05	19.11	0.81	0.39	0.24	1.030	0.030
250B			1	0.59	–	16.63	–	0.19	–	–	–
251	33226	HD 265866	12	0.27	0.04	13.06	0.68	0.24	0.86	1.085	0.091
273	36208		12	0.29	0.07	11.82	0.43	0.73	2.48	1.027	–
	36338		3	0.47	0.10	12.93	0.33	-0.88	2.62	–	–
	36834		8	0.42	0.04	15.26	0.73	0.03	0.50	0.977	–
	37217		1	0.23	–	11.65	–	-0.17	–	0.961	–
285	37766		3	11.94	1.88	18.27	0.55	1.23	0.81	–	–
2066	40501		7	0.49	0.07	16.28	0.90	-0.21	1.07	1.008	0.031
	41689		4	0.40	0.02	24.84	0.30	0.42	0.14	1.081	0.032
	42220		4	0.59	0.03	25.90	0.27	0.11	0.11	1.019	0.025
324B		HD 75732B	0	–	–	–	–	–	–	–	–
338A	45343	HD 79210	16	0.87	0.09	24.93	0.46	0.23	0.09	1.038	0.017
338B	120005	HD 79211	19	0.95	0.09	24.46	0.38	0.24	0.14	1.043	0.017
	46655		2	0.25	0.04	11.90	1.97	-0.47	1.99	–	–

Table 3—Continued

GJ	HIP	Other	# good spectra <sup>a</sup>	EW (Å)	$\sigma_{EW}$ (Å)	FWHM (km s <sup>-1</sup> )	$\sigma_{FWHM}$ (km s <sup>-1</sup> )	$\Delta\lambda_c$ (km s <sup>-1</sup> )	$\sigma_{\Delta\lambda_c}$ (km s <sup>-1</sup> )	V/R	$\sigma_{V/R}$
	46769		4	0.69	0.03	20.91	0.28	0.07	0.32	1.033	0.042
357	47103		5	0.18	0.02	12.42	1.41	-0.52	0.26	0.950	–
	47513		7	0.75	0.04	18.59	0.44	0.11	0.27	1.023	–
	47650		3	2.07	0.37	14.96	0.01	0.40	0.41	1.015	–
	48714		13	1.10	0.09	23.86	0.35	0.06	0.09	1.02	0.016
382	49986	SAO 137411	20	1.10	0.10	20.05	0.46	0.19	0.16	1.014	0.013
388		SAO 81292	0	–	–	–	–	–	–	–	–
390	51007		9	0.92	0.07	21.53	0.33	0.15	0.12	1.033	0.010
393	51317		18	0.47	0.06	15.51	0.50	0.15	0.29	1.021	0.021
394		HD 237903	2	0.73	0.03	26.58	0.00	0.22	0.13	1.055	0.030
	51468	HD 90875	13	0.26	0.03	32.59	0.44	0.16	0.09	1.048	0.029
397	51525		15	0.84	0.08	26.43	0.65	0.16	0.20	1.017	0.022
402	53020		0	–	–	–	–	–	–	–	–
406			3	16.22	5.29	12.56	0.33	0.21	1.03	0.991	–
408	53767		13	0.40	0.06	13.38	0.63	-0.19	0.94	1.014	0.008
410	53985	HD 95650	16	2.22	0.22	21.54	0.27	0.06	0.16	0.992	0.014
411	54035	HD 95735	30	0.14	0.03	14.60	0.44	0.54	0.47	–	–
412A	54211	SAO 43609	16	0.15	0.03	15.51	0.93	0.48	0.49	1.071	0.040
413	54532		9	0.44	0.05	17.49	0.74	0.38	0.39	0.999	0.012
414B		HD 97101B	5	0.84	0.04	22.38	0.62	0.38	0.22	1.071	0.015
414A	54646	HD 97101	20	0.62	0.08	27.18	0.66	0.16	0.15	1.036	0.022
424	55360	SAO 15475	9	0.44	0.04	21.14	1.02	0.49	0.62	1.037	0.025
433	56528	SAO 202602	4	0.33	0.02	19.67	0.96	0.43	0.38	1.088	0.054
	57050		1	0.28	–	11.09	–	-0.54	–	–	–
436	57087		51	0.31	0.03	15.98	0.57	0.18	0.53	1.008	0.064
445	57544		0	–	–	–	–	–	–	–	–

Table 3—Continued

GJ	HIP	Other	# good spectra <sup>a</sup>	EW (Å)	$\sigma_{EW}$ (Å)	FWHM (km s <sup>-1</sup> )	$\sigma_{FWHM}$ (km s <sup>-1</sup> )	$\Delta\lambda_c$ (km s <sup>-1</sup> )	$\sigma_{\Delta\lambda_c}$ (km s <sup>-1</sup> )	V/R	$\sigma_{V/R}$
447	57548		6	0.38	0.09	11.00	0.64	1.13	2.88	–	–
450	57802	SAO 43609	15	0.82	0.09	17.88	0.33	0.40	0.27	1.023	–
	59406B	L 758-107	0	–	–	–	–	–	–	–	–
465	60559		2	0.10	0.00	12.17	1.55	-4.35	6.95	–	–
486	62452		5	0.17	0.10	13.29	2.50	-1.11	2.88	1.059	0.025
	62687	HD 111631	11	1.02	0.06	25.18	0.38	0.13	0.11	1.023	0.012
494A	63510		2	5.21	0.16	22.98	0.39	0.90	12.48	–	–
514			26	0.65	0.08	20.79	0.32	0.30	0.14	1.039	0.020
	66459	SAO 63647	11	0.77	0.06	23.82	0.35	0.25	0.09	1.041	0.014
526	67155	HD 119850	17	0.44	0.06	19.45	0.58	0.35	0.19	1.034	0.023
	67164		3	0.23	0.03	11.45	0.63	1.84	1.91	–	–
	68469	HD 122303	12	0.58	0.09	20.88	0.42	0.38	0.28	1.040	0.034
	70865		5	0.45	0.06	21.27	0.83	0.38	0.35	1.060	0.043
	70975		1	0.16	–	13.29	–	-0.12	–	1.001	–
555	71253		7	0.33	0.04	12.11	0.81	0.05	0.70	1.016	–
9492	71898	SAO 17568	6	0.30	0.05	13.66	1.09	-0.66	1.06	1.046	–
569A	72944		1	3.74	–	17.72	–	0.19	–	–	–
581	74995		12	0.13	0.05	12.42	1.07	0.25	0.82	1.073	0.136
	79755	HD 147379A	16	0.86	0.08	26.40	0.28	0.21	0.14	1.028	0.023
		HD 147379B	11	0.63	0.08	16.73	0.42	-0.15	0.35	0.970	0.015
623	80346		1	0.19	–	11.67	–	6.48	–	–	–
625	80459		11	0.25	0.07	11.79	0.67	0.52	1.88	–	–
628	80824		19	0.32	0.06	11.84	0.59	-0.39	1.23	–	–
638	82003	HD 151288	22	0.62	0.06	26.48	0.42	0.28	0.05	1.053	0.019
649	83043		26	0.83	0.07	21.09	0.35	0.22	0.14	1.026	0.016
	83762		2	0.33	0.06	14.97	0.78	0.22	0.79	1.077	–

Table 3—Continued

GJ	HIP	Other	# good spectra <sup>a</sup>	EW (Å)	$\sigma_{EW}$ (Å)	FWHM (km s <sup>-1</sup> )	$\sigma_{FWHM}$ (km s <sup>-1</sup> )	$\Delta\lambda_c$ (km s <sup>-1</sup> )	$\sigma_{\Delta\lambda_c}$ (km s <sup>-1</sup> )	V/R	$\sigma_{V/R}$
	84099		13	0.41	0.14	13.22	0.93	0.36	1.03	1.018	0.066
667C			4	0.28	0.05	11.91	0.71	-0.45	0.92	–	–
	84790		8	0.26	0.02	12.81	0.70	0.00	1.01	1.063	0.078
673	85295	HD 157881	21	0.88	0.07	25.60	0.52	-0.33	0.06	0.963	0.016
678	85665	SAO 122446	17	0.65	0.09	21.41	0.51	0.25	0.14	1.032	0.025
687	86162	SAO 17568	26	0.34	0.05	13.50	0.56	0.20	0.67	–	–
686	86287		19	0.30	0.05	17.68	0.48	0.34	0.27	1.032	0.031
694	86776		19	0.51	0.11	15.34	0.61	0.51	0.59	–	–
2130A	86961		8	1.14	0.16	20.65	0.58	0.22	0.51	1.023	0.023
699	87937		34	0.22	0.07	10.10	0.50	0.18	1.53	1.015	–
701	88574	HD 165222	28	0.48	0.04	18.82	0.47	0.32	0.23	1.026	0.022
		LHS 462	3	0.20	0.03	11.45	1.40	0.89	0.12	1.033	–
		G 205-028	2	0.52	0.02	12.21	0.80	-1.93	5.02	–	–
4063			10	0.54	0.09	15.78	0.79	1.36	3.80	0.974	0.048
	91699		7	0.23	0.03	12.52	0.43	0.92	1.67	0.931	0.095
725A	91768	HD 173739	19	0.14	0.03	12.01	0.64	0.50	2.63	–	–
725B	91772	HD 173740	14	0.26	0.08	10.80	0.47	-0.35	0.49	–	–
729	92403		5	3.93	0.31	13.07	0.64	-2.22	1.84	–	–
745A	93873		2	–	–	11.63	1.57	-0.26	0.22	1.022	–
745B	93899	HD 349726	0	–	–	–	–	–	–	–	–
		G 207-019	2	0.33	0.12	11.08	1.58	-0.31	0.98	–	–
752A	94761	HD 180617	35	0.52	0.05	18.54	0.39	0.33	0.17	1.032	0.018
1245B			0	–	–	–	–	–	–	–	–
	99427	HD 193202	11	0.46	0.05	29.16	0.57	0.34	0.09	1.045	0.027
793	101180		9	0.84	0.09	12.92	0.28	0.23	0.71	–	–
806	102401		12	0.46	0.07	15.52	0.62	-0.09	0.64	1.036	0.034

Table 3—Continued

GJ	HIP	Other	# good spectra <sup>a</sup>	EW (Å)	$\sigma_{EW}$ (Å)	FWHM (km s <sup>-1</sup> )	$\sigma_{FWHM}$ (km s <sup>-1</sup> )	$\Delta\lambda_c$ (km s <sup>-1</sup> )	$\sigma_{\Delta\lambda_c}$ (km s <sup>-1</sup> )	V/R	$\sigma_{V/R}$
809	103096		20	0.76	0.06	23.23	0.35	0.29	0.08	1.052	0.016
	104432		7	0.16	0.03	12.44	0.54	-0.04	1.70	–	–
846	108782	HD 209290	18	0.94	0.09	23.38	0.48	0.18	0.09	1.030	0.019
849	109388		20	0.47	0.03	17.65	0.45	0.22	0.35	1.003	0.029
	109555		9	1.02	0.11	20.40	0.45	0.21	0.12	1.011	0.009
860A	110893	HD 239960	15	0.24	0.06	11.57	0.41	-0.55	2.22	1.005	0.003
873	112460		0	–	–	–	–	–	–	–	–
876	113020		108	0.38	0.08	12.68	0.51	0.13	1.76	1.027	0.033
880	113296	HD 216899	22	0.96	0.09	21.72	0.36	0.16	0.13	1.029	0.014
884	113576	HD 217357	40	0.79	0.06	25.06	0.46	0.16	0.09	1.029	0.013
887	114046	HD 217987	33	0.54	0.06	19.37	0.53	0.28	0.17	1.018	0.010
891	114411		3	0.55	0.08	15.51	0.56	-0.26	0.66	–	–
	115332		8	0.52	0.10	12.54	0.58	-0.11	1.83	–	–
	115562		3	1.08	0.12	22.17	0.54	0.21	0.10	1.044	0.054
905			2	1.59	0.28	11.10	0.01	0.08	3.62	–	–
908	117473	SAO 128397	27	0.20	0.03	15.15	0.53	0.29	0.62	1.049	0.012
911	117886		4	0.89	0.05	23.69	0.69	0.27	0.34	1.061	0.054

<sup>a</sup>Occasionally our automated process could not fit the line(s) in a spectrum, or the fit was of bad quality and had to be rejected. This column lists the number of spectra in which the K line was successfully fit for each star.

## REFERENCES

- Ayres, T. R. 1979, *ApJ*, 228, 509
- Bochanski, J. J., Hawley, S. L., Reid, I. N., Covey, K. R., West, A. A., Tinney, C. G., & Gizis, J. E. 2005, *AJ*, 130, 1871
- Burrows, A., Hubbard, W. B., Saumon, D., & Lunine, J. I. 1993, *ApJ*, 406, 158
- Burrows, A., et al. 1997, *ApJ*, 491, 856
- Butler, R. P., Marcy, G. W., Williams, E., McCarthy, C., Dosanjuh, P., & Vogt, S. S. 1996, *PASP*, 108, 500
- Caillault, J.-P. 1996, *ASP Conf. Ser. 109: Cool Stars, Stellar Systems, and the Sun*, 109, 325
- Cram, L. E., & Giampapa, M. S. 1987, *ApJ*, 323, 316
- Cram, L. E., & Mullan, D. J. 1979, *ApJ*, 234, 579
- Doyle, J. G., Houdebine, E. R., Mathioudakis, M., & Panagi, P. M. 1994, *A&A*, 285, 233
- Eason, E. L. E., Giampapa, M. S., Radick, R. R., Worden, S. P., & Hege, E. K. 1992, *AJ*, 104, 1161
- ESA, . 1997, *VizieR Online Data Catalog*, 1239, 0–+
- Fleming, T. A., Schmitt, J. H. M. M., & Giampapa, M. S. 1995, *ApJ*, 450, 401
- Giampapa, M. S. 1994, *ASP Conf. Ser. 64: Cool Stars, Stellar Systems, and the Sun*, 64, 509
- Giampapa, M. S., Cram, L. E., & Wild, W. J. 1989, *ApJ*, 345, 536
- Giampapa, M. S., Worden, S. P., & Linsky, J. L. 1982, *ApJ*, 258, 740
- Gizis, J. E. 1997, *AJ*, 113, 806
- Gizis, J. E., Reid, I. N., & Hawley, S. L. 2002, *AJ*, 123, 3356
- Hawley, S. L., et al. 2003, *ApJ*, 597, 535
- Hünsch, M., Schmitt, J. H. M. M., Sterzik, M. F., & Voges, W. 1999, *A&AS*, 135, 319
- Johns-Krull, C. M., & Valenti, J. A. 1996, *ApJ*, 459, L95
- Liebert, J. 1994, *ASP Conf. Ser. 64: Cool Stars, Stellar Systems, and the Sun*, 64, 520
- Mathioudakis, M., & Doyle, J. G. 1991, *A&A*, 244, 409

- Mullan, D. J., & Fleming, T. A. 1996, *ApJ*, 464, 890
- Panagi, P. M., & Mathioudakis, M. 1993, *A&AS*, 100, 343
- Reid, N., Hawley, S. L., & Mateo, M. 1995, *MNRAS*, 272, 828
- Reid, I. N., Kirkpatrick, J. D., Liebert, J., Gizis, J. E., Dahn, C. C., & Monet, D. G. 2002, *AJ*, 124, 519
- Robinson, R. D., Cram, L. E., & Giampapa, M. S. 1990, *ApJS*, 74, 891
- Robrade, J., & Schmitt, J. H. M. M. 2005, *A&A*, 435, 1073
- Rutten, R. G. M., Zwaan, C., Schrijver, C. J., Duncan, D. K., & Mewe, R. 1989, *A&A*, 219, 239
- Schrijver, C. J., & Rutten, R. G. M. 1987, *A&A*, 177, 143
- Short, C. I., & Doyle, J. G. 1998, *A&A*, 336, 613
- Shkolnik, E., Walker, G. A. H., Rucinski, S. M., Bohlender, D. A., & Davidge, T. J. 2005, *AJ*, 130, 799
- Smith, G. H., & Shetrone, M. D. 2004, *PASP*, 116, 604
- Stauffer, J. R., Hartmann, L. W., Prosser, C. F., Randich, S., Balachandran, S., Patten, B. M., Simon, T., & Giampapa, M. 1997, *ApJ*, 479, 776
- Valenti, J. A., & Johns-Krull, C. M. 2003, *IAU Symposium*, 219, 235
- Veeder, G. J. 1974, *AJ*, 79, 1056
- Vogt, S. S., Allen, S. L., Bigelow, B. C., Bresee, L., Brown, B., Cantrall, T., Conrad, A., Couture, M., Delaney, C., Epps, H. W., Hilyard, D., Hilyard, D. F., Horn, E., Jern, N., Kanto, D., Keane, M. J., Kibrick, R. I., Lewis, J. W., Osborne, J., Pardeilhan, G. H., Pfister, T., Ricketts, T., Robinson, L. B., Stover, R. J., Tucker, D., Ward, J., & Wei, M. Z. 1994, In *Proc. SPIE Instrumentation in Astronomy VIII*, David L. Crawford; Eric R. Craine; Eds., Volume 2198, p. 362, pp. 362–+
- Wright, J. T., Marcy, G. W., Butler, R. P., & Vogt, S. S. 2004, *ApJS*, 152, 261